Chapter III - IOPs in seawater

A) Absorption

The main constituents of seawater are usually:

- water molecules (absorption by salts is often neglected or included in the dissolved phase)
- phytoplankton
- dissolved organic matter (DOM)
- detritus
- sediments

Based on the assumption of linearity of optical phenomena, the absorption can be broken down into the sum of the absorptions by these different constituents:

$a = a_w + a_{phi} + a_{DOM} + a_{det} + a_{sed}$

Sediments are usually considered as suspended inorganic particles for which absorption can be neglected.

The is also another classification being used:

$a = a_w + a_P + a_{ds}$

$a = a_w + (a_{phy} + a_{nap}) + a_{ds}$

where P = particles [this category can be split into phy (algae) and NAP (Non Algal Particles)] and ds = dissolved.

Note: **This classification is preferable to the preceding one as detritus can have particular and dissolved components.**

1) Absorption by pure water

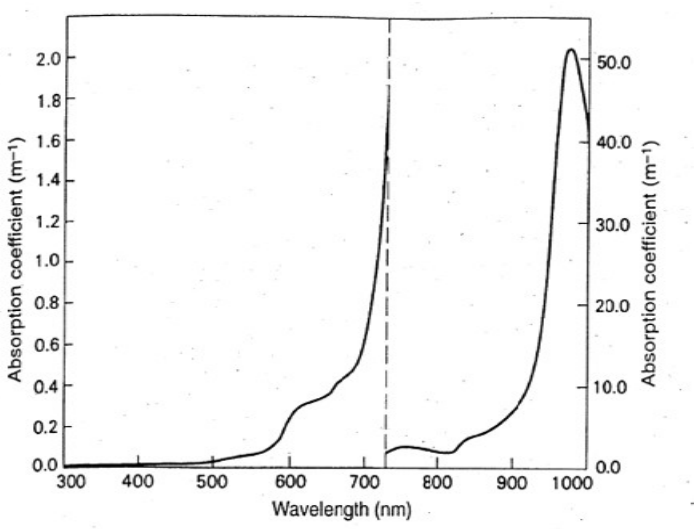

Fig. 3.3. Absorption spectrum of pure water. Absorption coefficient values have been taken from Table 3.1 for the range 310–790 nm, and from the data of Palmer & Williams (1974) for the range 790–1000 nm.

Light and Photosynthesis in Aquatic Ecosystems
John T.O. Kirk, 1983
Cambridge Univ Press
Fig 3.3
(2nd edition, 1994)

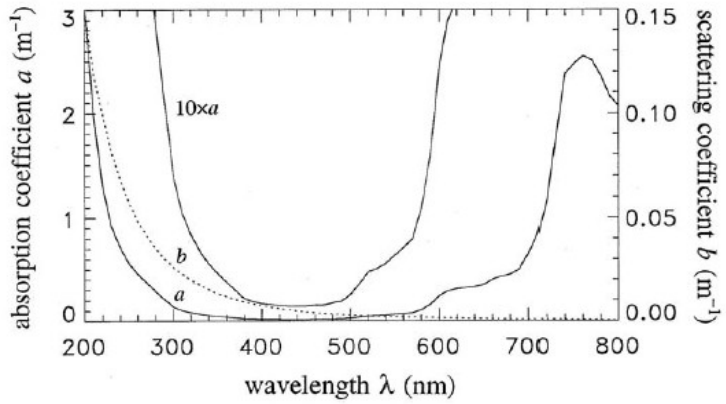

Fig. 3.6. Absorption (solid line) and scattering (dotted line) coefficients for pure sea water, as determined by Smith and Baker (1981).

(Courtesy, Mobley, Light and Water, 1994, Fig 3.6)

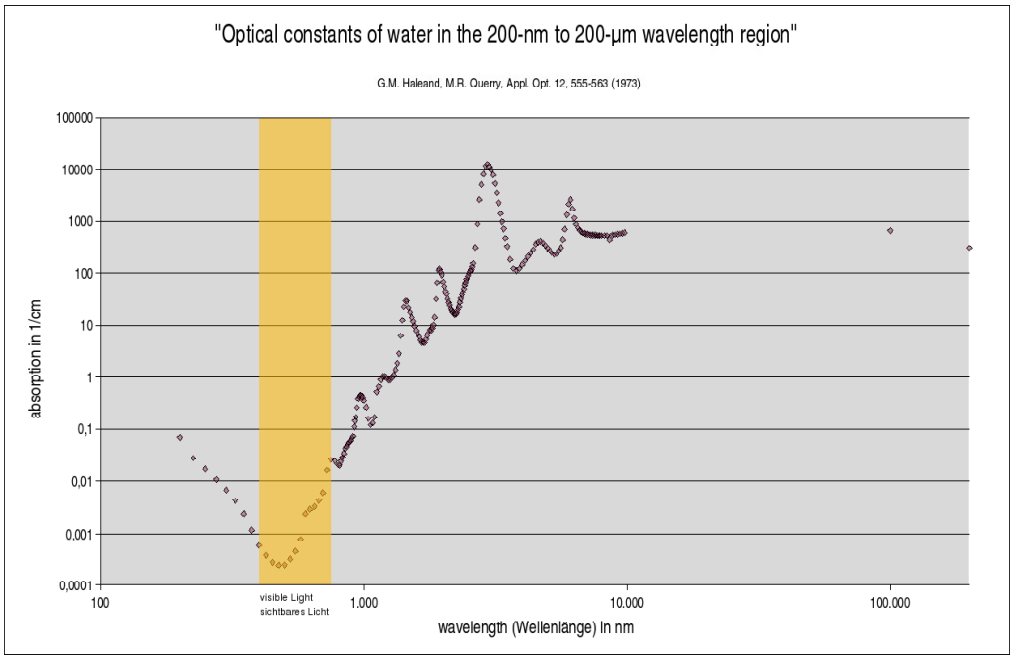

Absorption coefficient of water in cm^{-1}. (G.M. Haleand, M.R. Querry, Optical constants of water in the 200-nm to 200-µm wavelength region, Appl. Opt. 12, 555-563, 1973).

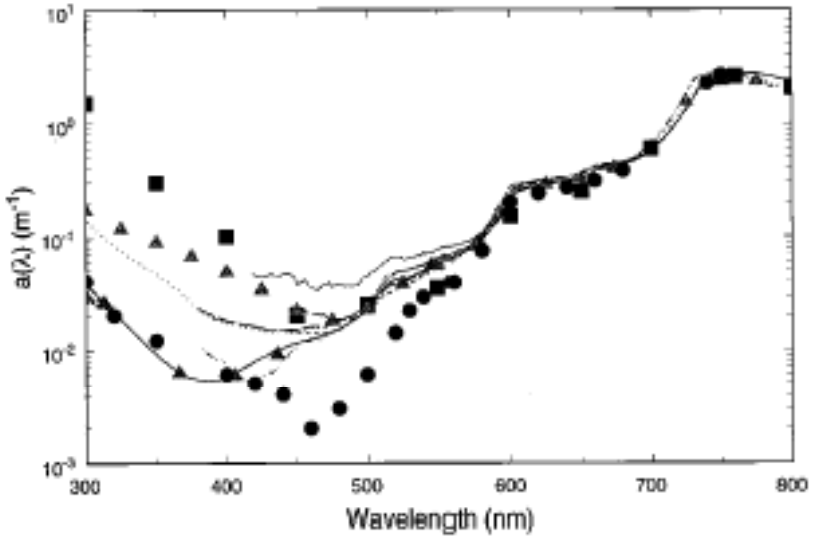

Fig. 1. Absorption coefficient of pure water as measured or compiled by several investigators.[1,2,11,18,19,21,26–33] The discrepancy in the estimated absorption coefficients is largest at short wavelengths where absorption by organic contaminants is significant. At wavelengths longer than 550 nm the standard deviation of the estimates is between 5 and 10% of the mean value.

Pegau et al, Applied Optics 97 (Pegau, W.S., Gray, D. and Zaneveld, J.R.V. (1997) Absorption and Attenuation of Visible and Near-Infrared Light in Water: Dependence on Temperature and Salinity. Applied Optics, 36, 6035. http://dx.doi.org/10.1364/AO.36.006035

Note: The differences are methodological

The values currently in use are those by Pope and Fry (Robin M. Pope and Edward S. Fry, "Absorption spectrum (380–700 nm) of pure water. II. Integrating cavity measurements," Appl. Opt. **36**, 8710-8723, 1997).

2) Absorption by pigments

A) Chlorophyll

Chlorophyll (word created in 1817 from khloros which is Greek for pale green and phyllon which means leaf) is the main pigment used for photosynthesis in higher plants.

Isolated in 1817 by Joseph Bienaimé Caventou, this pigment, located in the chloroplasts of plant cells, is involved in photosynthesis to convert light energy into chemical energy. Its absorption spectrum of light is responsible for the green colour of plants: green wavelengths are least absorbed and are largely reflected which is what we see with our eyes.

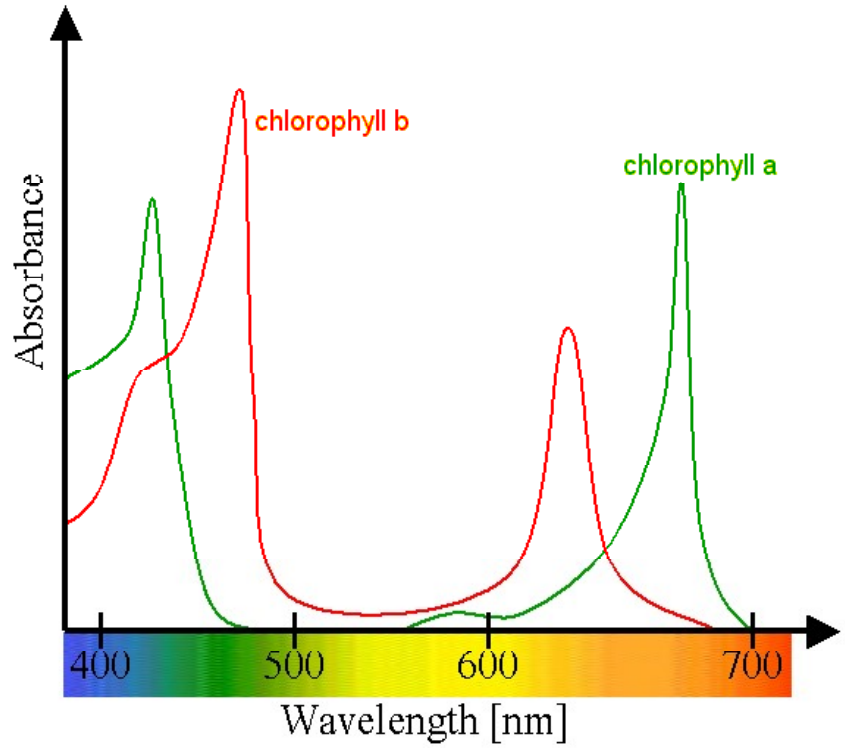

Absorption spectra for chlorophyll *a* (green) and chlorophyll *b* (red) (Source Garcia; Nashev). Note: Light perceived as "green" by the human eye and brain has a wavelength approximately between 490 and 570 nm (unlike the colour bar shown above).

There are different types of chlorophyll based on their chemical structure:

* "Chlorophyll *a*" (symbol: "chla") is the most common photosynthetic pigment in the plant kingdom; it is present in all aquatic and terrestrial plants (≈ 2 g/kg of fresh leaves). The measurement of its concentration in water is used as an indicator of the quantity of phytoplankton (at the base of the aquatic food web). Chlorophyll concentrations in water are usually given in µg chla/L;
* "Chlorophyll *b*" is found in Cormophytes (higher plants) and Chlorophyceae (green algae) at lower levels (≈ 0.75 g/kg);

There are two more less abundant variants:
* Chlorophyll *c* (C1 and C2) found in phaeophyceae (called brown algae);
* Chlorophyll *d* found in certain cyanobacteria (sometimes called blue algae).

The radiometric analysis of the luminance (at various wavelengths) emanating from the ocean surface makes it possible to determine the chlorophyll concentration (see last chapter).

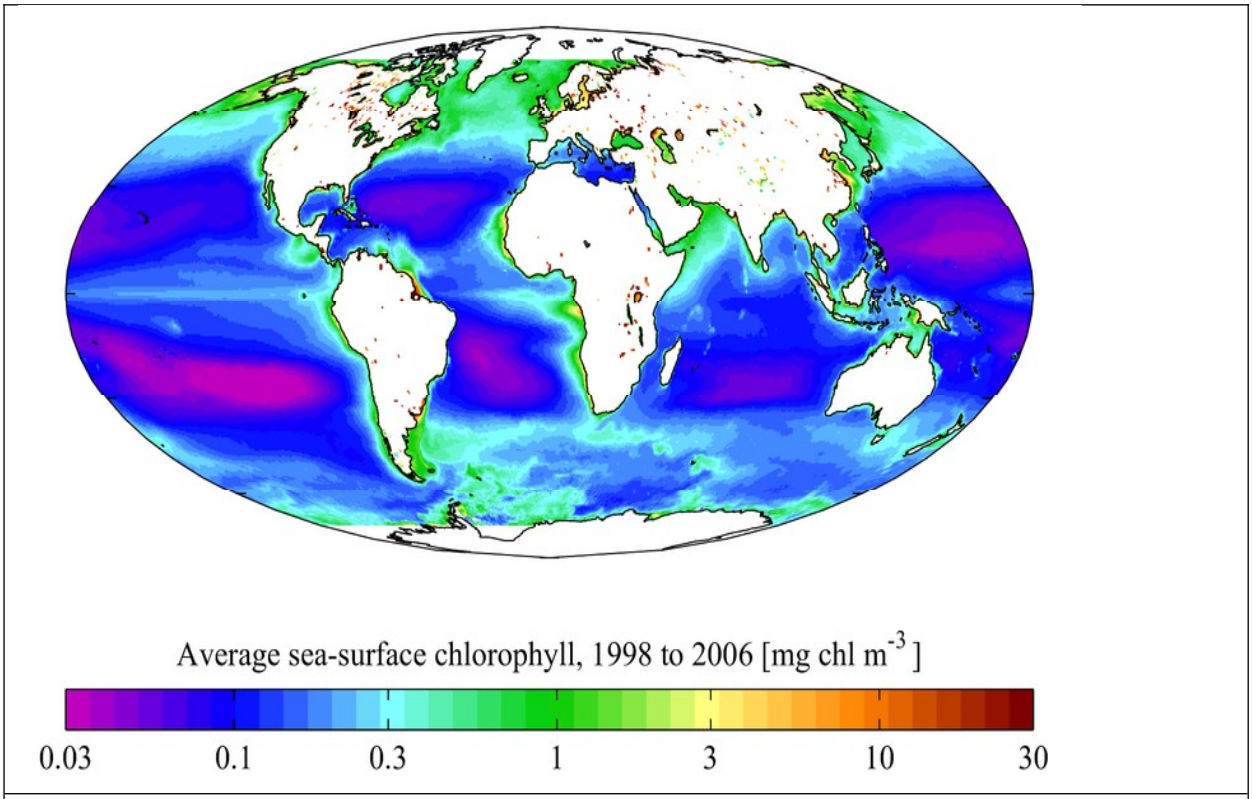

Average chlorophyll content of marine surface waters (from SeaWIFS) for the period 1998-2006 (logarithmic scale).

Chemical structure

Chlorophyll is a chlorine (four pyrrole rings in a circle), chelating* a magnesium atom in the centre, as well as a long chain alcohol, phytol (except for chlorophyll *c*). It has a structure almost identical to heme (present in red blood cells). The presence of numerous **conjugated double bonds** in its structure allows for interactions with (and the absorption of) light. The side chains of chlorine are variable which leads to a modification of the absorption spectrum between the different types of chlorophyll.

(*Note [source Wikipedia]: chelation (from Greek χηλή, chēlē, meaning "claw") is a type of bonding of ions and molecules to metal ions. It involves the formation or presence of two or more separate coordinate bonds between a polydentate (multiple bonded) ligand and a single central atom. These ligands are called chelants, chelators, chelating agents, or sequestering agents. They are usually organic compounds, but this is not a necessity.

The term chelate was first applied in 1920 by Sir Gilbert T. Morgan and H. D. K. Drew, who stated: "The adjective chelate, derived from the great claw or chele (Greek) of the lobster or other crustaceans, is suggested for the caliperlike groups which function as two associating units and fasten to the central atom so as to produce heterocyclic rings.".)

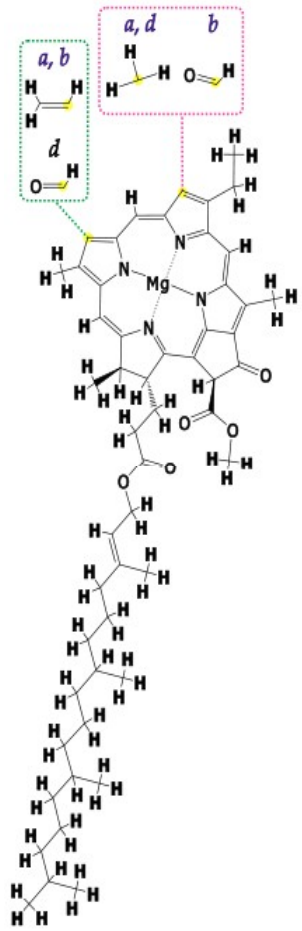

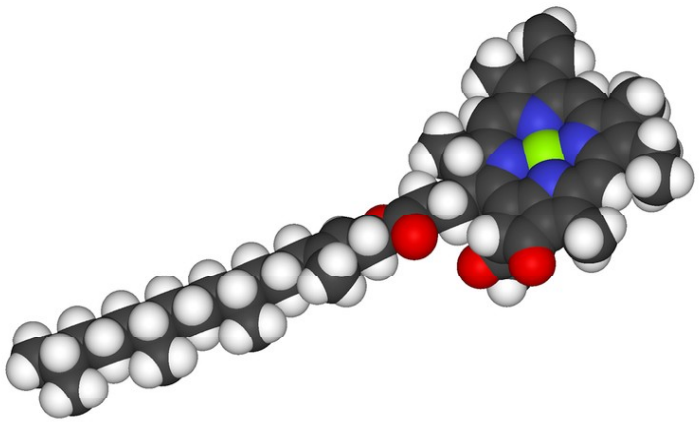

Top: Chlorophyll molecule showing the magnesium atom in green, nitrogen in blue, and oxygen in red.

Left: Classical structure of chlorophyll *a*, *b* and *d.*

B) Carotenoids

Carotenes and xanthophylls are grouped together under the term carotenoids.

Carotenoids are mostly orange and yellow pigments that are ubiquitous in a large number of living organisms. Being liposoluble, they are typically easily assimilated by an organism. They are synthesized by all algae, all green plants, and by many fungi and bacteria (including cyanobacteria). They are absorbed by animals through their food.

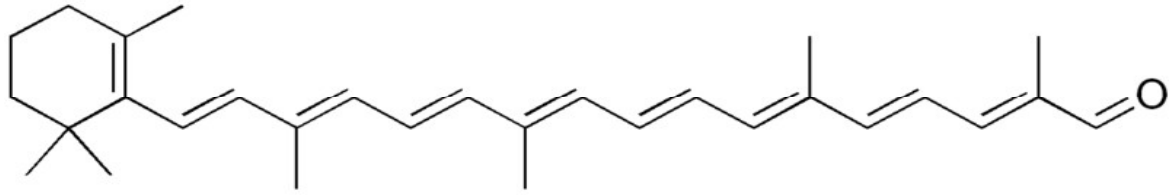

Structure of apocarotenal, a derivative of carotenoid. (Edgar)

C) Phycobiliproteins

Phycobiliproteins are water-soluble pigments used for photosynthesis. There are four types:

* Allophycocyanin (APC)
* C-Phycocyanin (CPC)
* B-Phycoerythrin (B-PE)
* Phycoerythrobilin

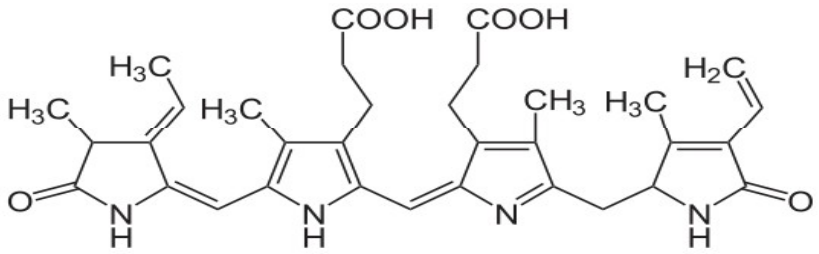

Phycoerythrobilin is one of the chromophores of phycoerythrin (source: NEUROtiker).

IMPORTANT:

In all these pigments, it is the presence of conjugated double or triple bonds that allows the absorption of photons.

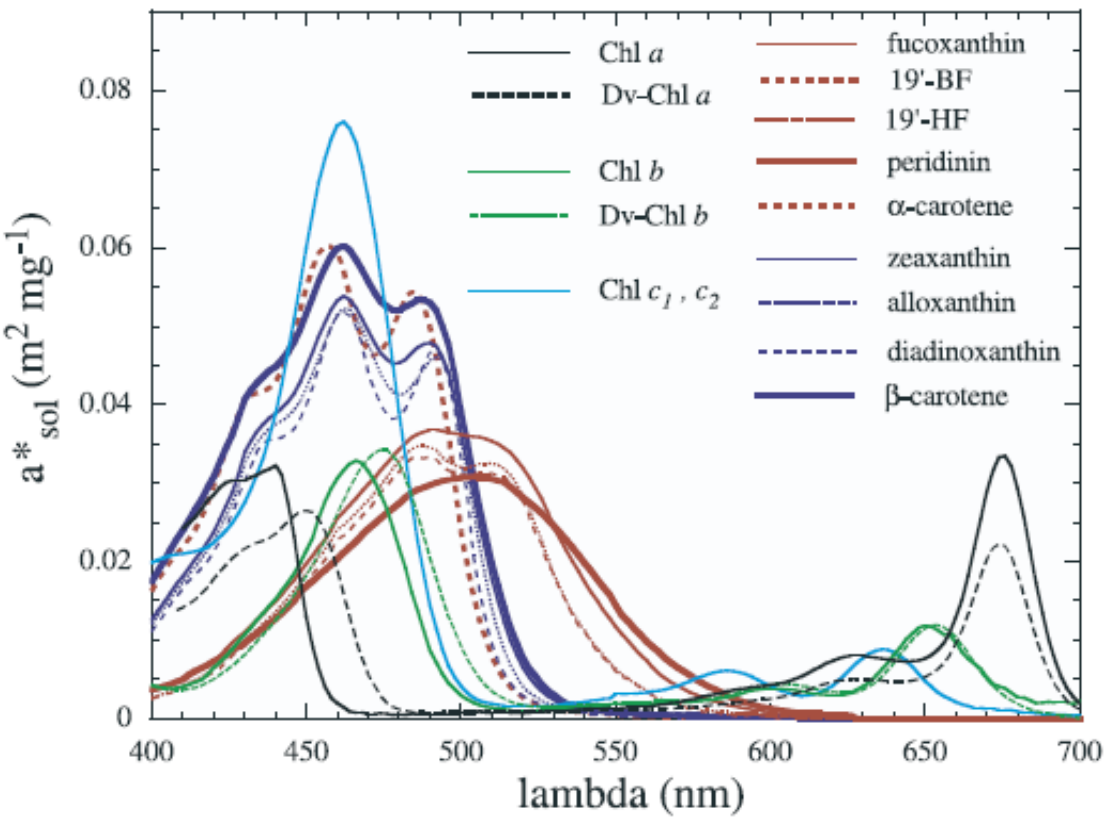

Figure 1. Assumed in vivo weight-specific absorption spectra of the main pigments, $a^*_{sol,i}(\lambda)$ (in m^2 mg^{-1}), as derived from absorption spectra of individual pigments in solvent (see text). Absorption spectra of photosynthetic and nonphotosynthetic carotenoids are shown in red and blue, respectively.

Bricaud et al., 2004 -Absorption spectra of the main pigments
(Bricaud, Annick & Claustre, Hervé & Ras, Joséphine & Oubelkheir, K. (2004). Natural variability of phytoplanktonic absorption in oceanic waters: Influence of the size structure of algal populations. Journal of Geophysical Research-Oceans. 109. 10.1029/2004jc002419.)

3) DOM Dissolved organic matter

The absorption of dissolved organic matter is modelled in the same way as for non-algal particles, using an exponential model:

$$a_{CDOM}(\lambda) = a_{CDOM}(\lambda_o) \exp(-S(\lambda - \lambda_o))$$

where λ_o is a reference wavelength (usually 440 nm) and S is the slope which is usually taken as 0.014 +/- 0.0032 nm^{-1} (Bricaud *et al.* 1981) or 0.016 nm^{-1} (Morel *et al.* 2007b).

There exists an uncertainty about the variability of absorption in coloured dissolved organic matter (CDOM). This can significantly affect the bio-optical algorithms used to estimate the concentration of Chl from remote sensing measurements (Siegel *et al.* 2005; Morel and Gentili 2009).

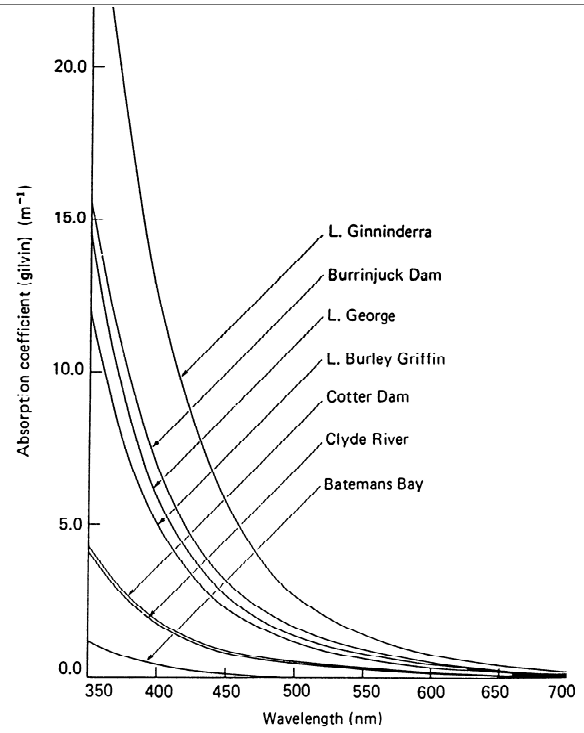

Kirk 1983

John T. O. *Kirk*: *Light and photosynthesis* in aquatic ecosystems.–With 108 figs, 401 pp. Cambridge–London–New York: Cambridge University Press *1983*.

4) Non-algal particles (referring to the particular components of what used to be called detritus)

By "non-algal particles" (NAP) we denote the poorly pigmented and non-pigmented particles derived from phytoplankton and various heterotrophs and bacteria (Bricaud et Stramski 1990). NAP also contribute to absorption, ranging from 10^{-3} to10^{-1} m^{-1} in oligotrophic environments which is of the same order of magnitude as the absorption by phytoplankton. lise NAP are also modelled using an exponential (Yentsch 1962 ; Kirk 1980 ; Roesler *et al.* 1989 ; Bricaud et Stramski 1990 ; Bricaud *et al.* 1998):

$$a_{NAP}(\lambda) = a_{NAP}(\lambda_o) \exp(-S(\lambda - \lambda_o))$$

where λ_o is again a reference wavelength (usually 440 nm) and S the slope of the spectral dependace, the mean value of which is usually 0.011 nm^{-1} (Roesler *et al.* 1989; Bricaud *et al.*, 1998).

5) Inorganic matter – mineral particles – sediments, atmospheric dust

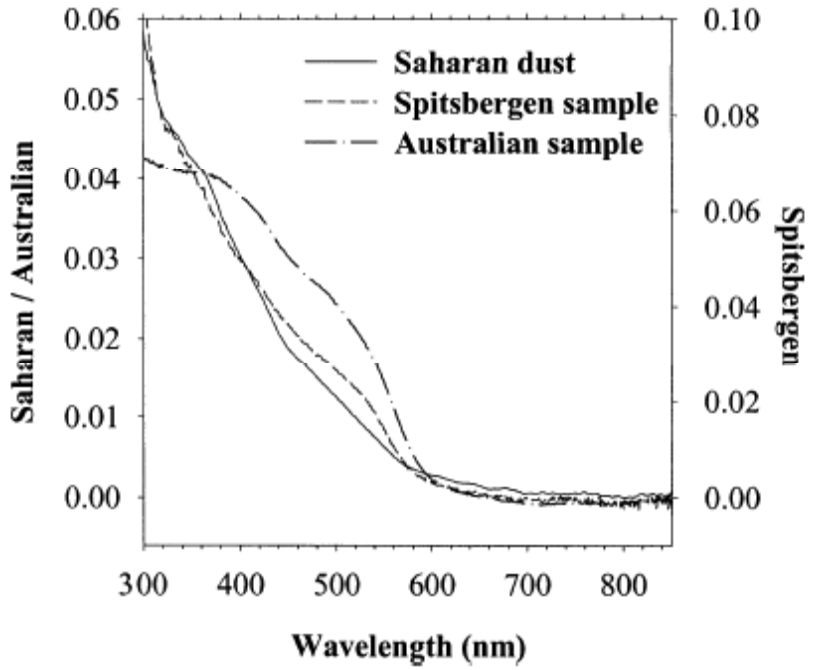

Fig. 5. Absorbance spectra of natural assemblages of mineral particles from three different environments.

Babin and Stramski 2004

Babin, M., and D. Stramski (2004), Variations in the mass-specific absorption coefficient of mineral particles suspended in water, Limnol. Oceanogr., 49(3), 756–767, doi:*10.4319/lo.2004.49.3.0756*.

The total absorption is thus the sum of the absorptions by all constituents.

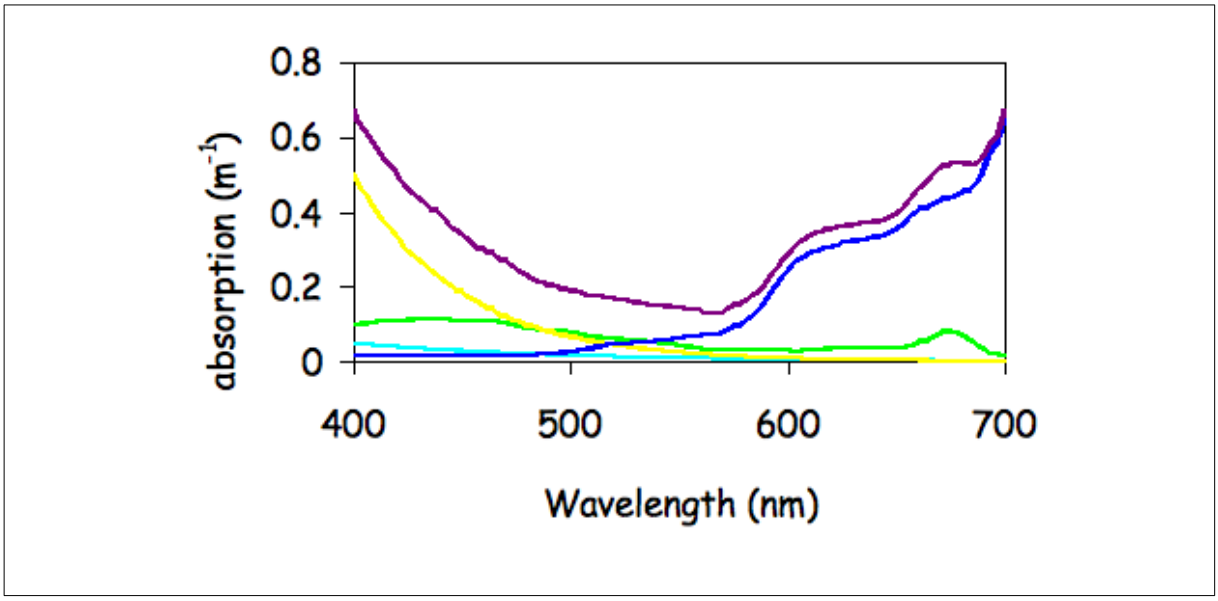

blue=water; green=phyto; yellow=CDOM; cyan= NAP;
purple=total absorption (courtesy: C. Roesler)

Fig Component and total absorption spectra for A. clear open ocean waters where water dominates the absorption and B. eutrophic coastal waters where particulate and dissolved organic matter dominate the blue and green portions of the spectrum.

blue=water; green= phyto; orange=CDOM; cyan= NAP; black= total absorption

(Courtesy C. Roesler ; http://www.oceanopticsbook.info/view/absorption/definitions)

Modelling: For oligotrophic waters, different formulas make it possible to calculate the total absorption from the chlorophyll concentration. Morel's model (1991) uses a simplified version of the formula from Prieur and Sathyendranath (1981).

$$a(\lambda) = \left[a_w(\lambda) + 0.06\, a_c^{*\prime}(\lambda)\, C^{0.65}\right]\left[1 + 0.2 \exp\left(-0.014(\lambda - 440)\right)\right]. \quad (3.27)$$

Here $a_w(\lambda)$ is the absorption coefficient of pure water and $a_c^{*\prime}(\lambda)$ is a nondimensional, statistically derived chlorophyll-specific absorption coefficient; $a_w(\lambda)$ and $a_c^{*\prime}(\lambda)$ values are given in Table 3.7 [these $a_w(\lambda)$ values are slightly different than those of Table 3.5]. When C is expressed in mg m^{-3} and λ is in nm, the resulting $a(\lambda)$ is in m^{-1}. Figure 3.10 shows $a(\lambda)$ as predicted by Eq. (3.27) for various chlorophyll concentrations. The predicted $a(\lambda)$ values are qualitatively similar to the measured $a(\lambda)$ of Fig. 3.9(a), although the magnitudes sometimes differ, especially for the higher chlorophyll concentrations.

Table 3.7. Absorption by pure sea water, a_w, and the nondimensional chlorophyll-specific absorption coefficient, $a_c^{*\prime}$, for use in Eq. (3.27).[a]

λ (nm)	a_w (m^{-1})	$a_c^{*\prime}$	λ (nm)	a_w (m^{-1})	$a_c^{*\prime}$	λ (nm)	a_w (m^{-1})	$a_c^{*\prime}$
400	0.018	0.687	500	0.026	0.668	600	0.245	0.236
410	0.017	0.828	510	0.036	0.618	610	0.290	0.252
420	0.016	0.913	520	0.048	0.528	620	0.310	0.276
430	0.015	0.973	530	0.051	0.474	630	0.320	0.317
440	0.015	1.000	540	0.056	0.416	640	0.330	0.334
450	0.015	0.944	550	0.064	0.357	650	0.350	0.356
460	0.016	0.917	560	0.071	0.294	660	0.410	0.441
470	0.016	0.870	570	0.080	0.276	670	0.430	0.595
480	0.018	0.798	580	0.108	0.291	680	0.450	0.502
490	0.020	0.750	590	0.157	0.282	690	0.500	0.329
						700	0.650	0.215

[a] Condensed with permission from Prieur and Sathyendranath (1981), who give values every 5 nm.

The results for this formula and difference chlorophyll concentrations are shown below (the table above and the following figure were taken from "Light and Water, Radiative transfer in

Natural Waters", Curt Mobley, Academic Press 1994).

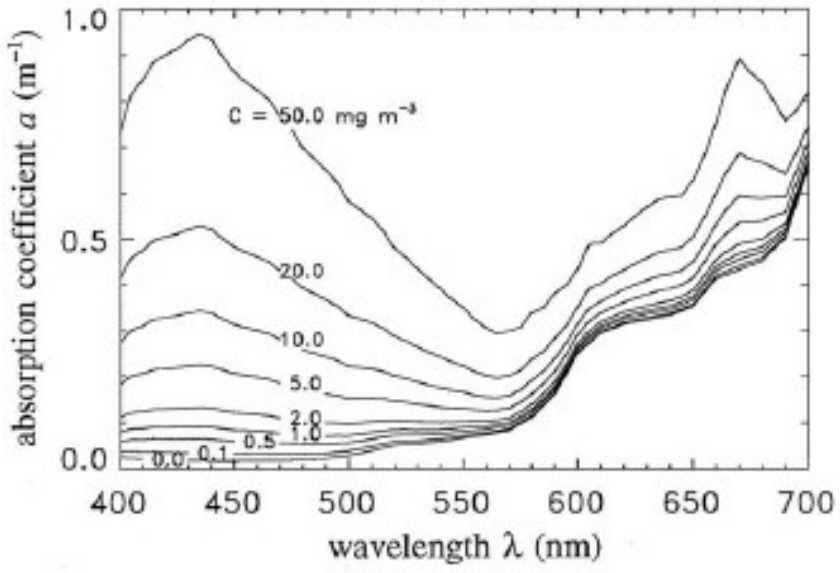

Fig. 3.10. Total spectral absorption coefficient $a(\lambda)$ for selected chlorophyll concentrations C, as predicted by Eq. (3.27).

Currently, and taking into account the constant technological advancement in the optical instruments (see Chapter VII) measuring IOPs, we often use the method in reverse, i.e., we determine the chlorophyll concentration from absorption measurements (e.g., Boss et al., 2007 from absorption by particulate matter):

$$A_{\Phi}(676)=[A_P(676)-\frac{39}{65}A_P(650)-\frac{26}{65}A_P(715)](m^{-1})$$

$$C_a=157\,A_{\Phi}(676)^{1.22}(mg\,m^{-3})$$

Boss, E.S., Collier, R., Larson, G., Fennel, K., Pegau, W.S., 2007. Measurements of spectral optical properties and their relation to biogeochemical variables and processes in Crater Lake, Crater Lake National Park, OR. Hydrobiol. 574, 149–159.

B) Scattering

Scattering is the excitation of a molecule and subsequent re-emission of electromagnetic energy in different directions. It depends on the size of the particle, its absorption, its refractive index, and the angle of incidence of light.

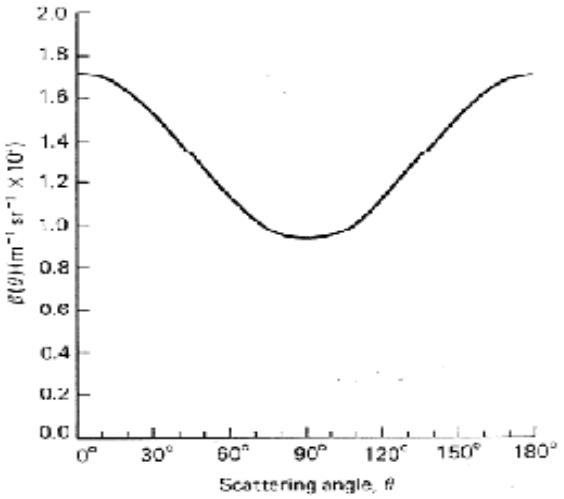

Fig. 4.8. Volume scattering function of pure water for light of wav 550 nm. The values are calculated on the basis of density fluc scattering, assuming that $\beta(90°) = 0.93 \times 10^{-4}$ m^{-1} sr^{-1} an $\beta(\theta) = \beta(90°)(1 + 0.835 \cos^2 \theta)$ (following Morel, 1974).

Scattering by pure water (Morel, 1974) is very similar to Rayleigh scattering.

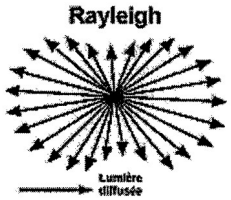

left
Kirk 1983, 1994

Equation representing the scattering in pure water (salinity from 35 to 39) (from "Light and Water, Radiative transfer in Natural Waters", Curt Mobley, Academic Press 1994)
Note: the equation is identical for pure sea water with different VSF(90°, λ_0) (see Table on following page)

$$\beta_w(\psi;\lambda) = \beta_w(90°;\lambda_o)\left(\frac{\lambda_o}{\lambda}\right)^{4.32}(1 + 0.835\cos^2\psi) \quad (m^{-1}\ sr^{-1}). \quad (3.28)$$

This equation is reminiscent of the form

$$\beta_{Ray}(\psi;\lambda) = \beta_{Ray}(90°;\lambda_o)\left(\frac{\lambda_o}{\lambda}\right)^{4}(1 + \cos^2\psi) \quad (m^{-1}\ sr^{-1}), \quad (3.29)$$

which is commonly called Rayleigh scattering. The wavelength dependence of $\lambda^{-4.32}$ (rather than λ^{-4}) results from the wavelength dependence of the index of refraction. The 0.835 factor (rather than 1) is attributable to the anisotropy of the water molecules.

The phase function corresponding to Eq. (3.28) is

$$\tilde{\beta}_w(\psi) = 0.06225\,(1 + 0.835\cos^2\psi) \quad (sr^{-1}), \quad (3.30)$$

and the total scattering coefficient $b_w(\lambda)$ is given by

$$b_w(\lambda) = 16.06\left(\frac{\lambda_o}{\lambda}\right)^{4.32}\beta_w(90°;\lambda_o) \quad (m^{-1}). \quad (3.31)$$

Table 3.8 gives values of $\beta_w(90°;\lambda)$ and $b_w(\lambda)$ for selected wavelengths, for both pure water and pure sea water ($S = 35$–$39‰$). Note that the pure sea water values are about 30% greater than the pure water values,

Table accompanying the scattering equation for pure water and pure sea water (salinity from 35 to 39) (from "Light and Water, Radiative transfer in Natural Waters", Curt Mobley, Academic Press 1994).

Table 3.8. The volume scattering function at $\psi = 90°$, $\beta(90°;\lambda)$, and the scattering coefficient $b(\lambda)$ for pure water and for pure sea water ($S = 35$-39‰). All numbers in the body of the table are times 10^{-4}, as shown in the first row.[a]

	pure water		pure sea water	
λ (nm)	$\beta_w(90°)$ (m^{-1} sr^{-1})	b_w[b] (m^{-1})	$\beta_{sw}(90°)$ (m^{-1} sr^{-1})	b_{sw}[b] (m^{-1})
350	6.47×10^{-4}	103.5×10^{-4}	8.41×10^{-4}	134.5×10−4
375	4.80	76.8	6.24	99.8
400	3.63	58.1	4.72	75.5
425	2.80	44.7	3.63	58.1
450	2.18	34.9	2.84	45.4
475	1.73	27.6	2.25	35.9
500	1.38	22.2	1.80	28.8
525	1.12	17.9	1.46	23.3
550	0.93	14.9	1.21	19.3
575	0.78	12.5	1.01	16.2
600	0.68	10.9	0.88	14.1

[a] Reproduced from Morel (1974), with permission.
[b] Computed from $b(\lambda) = 16.0\ \beta(90°;\lambda)$.

The latest internationally accepted values for scattering in pure sea water can be found in the article by Zhang et al., 2019.
X. Zhang, L. Hu, and M.-X. He, "Scattering by pure seawater: effect of salinity," Opt. Express 17, 5698–5710 (2009).

Scattering by sea water ("non-pure")
Scattering in sea water greatly depends on on the content of the water. Petzold (1972) was the first to perform measurements (Petzold, T.J., 1972. Volume scattering functions for selected ocean waters. *Scripps Inst. Oceanogr.* Report SIO 72-78). It took another 20 years before others rose to the technological challenge of building instruments capable of measuring scattering.

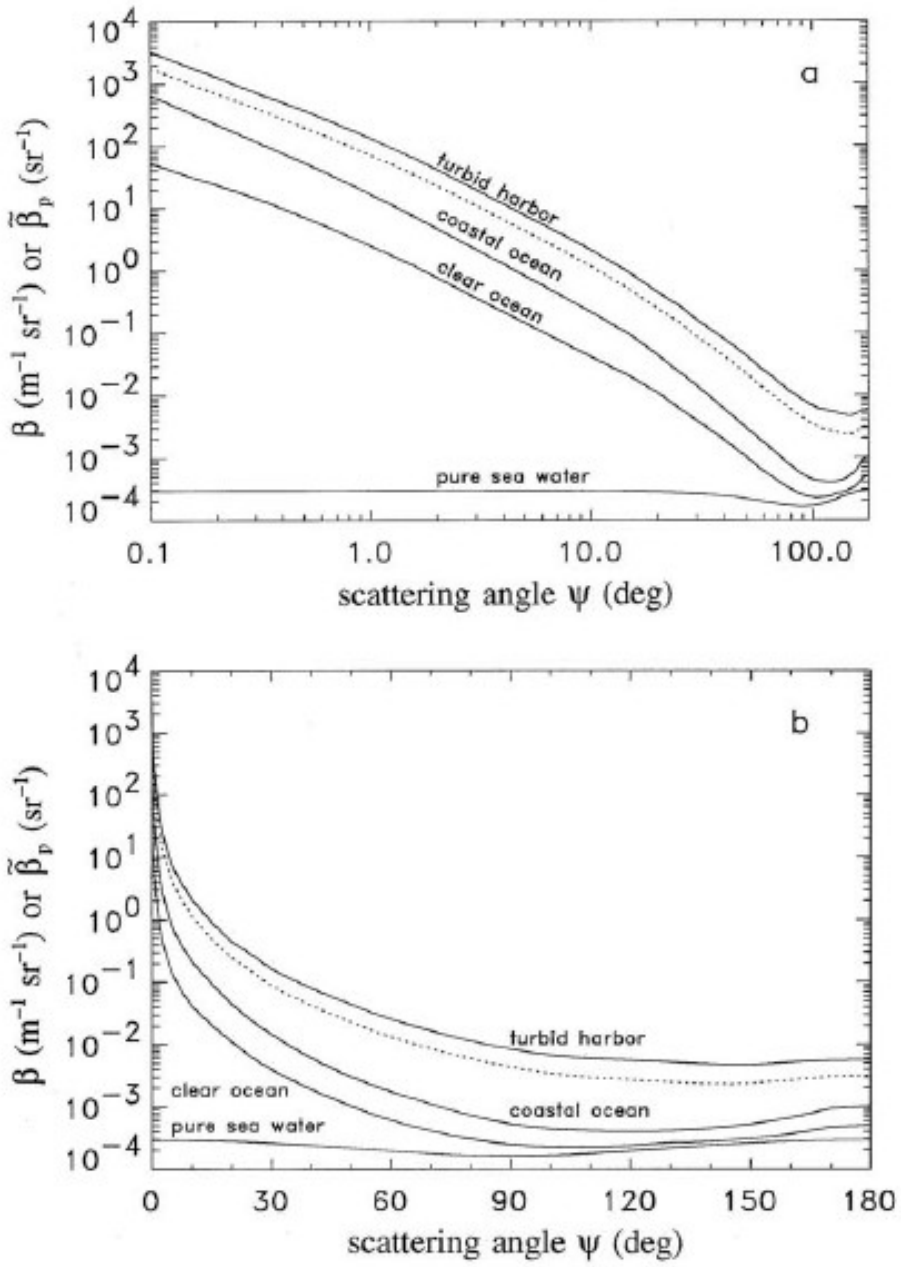

Fig. 3.13. Measured volume scattering functions β (solid lines) from three different natural waters, and the computed volume scattering function for pure sea water, all at $\lambda = 514$ nm. The dotted line is the particle phase function $\tilde{\beta}_p$ of Table 3.10. [redrawn from Petzold (1972)]

(Fig. from "Light and Water, Radiative transfer in Natural Waters", Curt Mobley, Academic Press 1994)

62 example phase functions measured in coastal waters off New Jersey (Boss and Lewis)
Note: although the phase function by Petzold for an average particle may seem like a good fit to the ensemble, it may be problematic to use it to represent individual measurements.

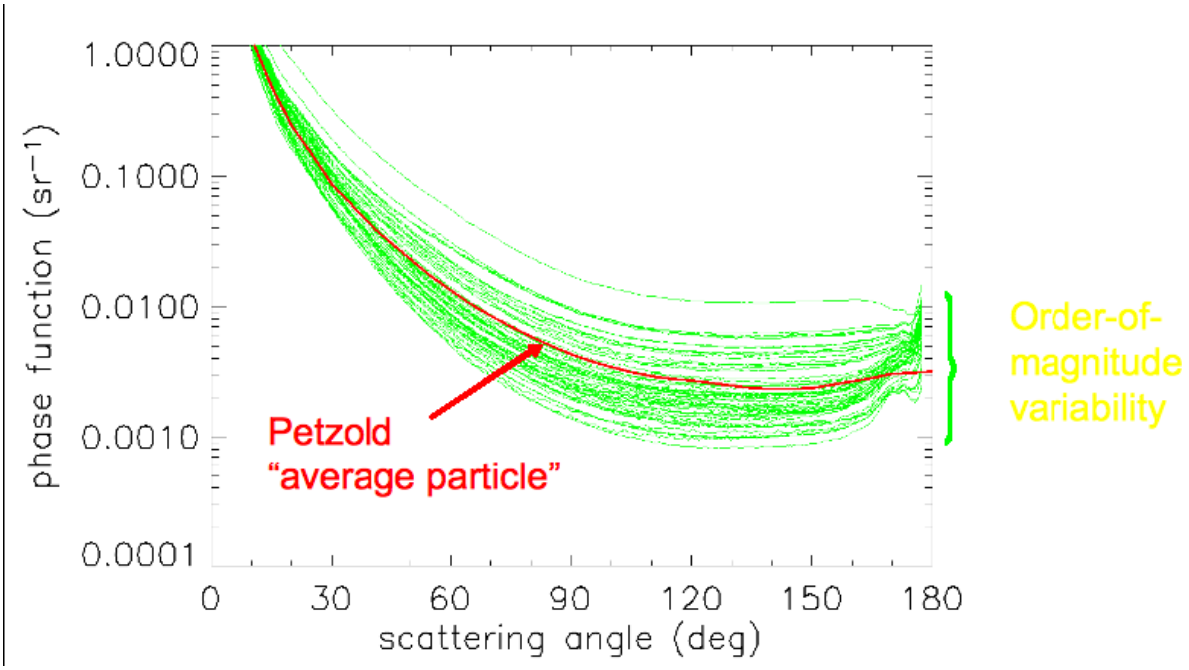

It is useful to have an analytical representation of these curves (Henyey-Greenstein, 1941):

$$\tilde{\beta}_{HG}(g;\psi) \equiv \frac{1}{4\pi} \frac{1 - g^2}{(1 + g^2 - 2g\cos\psi)^{3/2}}. \qquad (3.34)$$

Here g is a parameter that can be adjusted to control the relative amounts of forward and backward scattering in $\tilde{\beta}_{HG}$. Note that $\tilde{\beta}_{HG}$ satisfies the normalization condition (3.8) for any g.

The physical interpretation of g comes from noting that

$$2\pi \int_{-1}^{1} \tilde{\beta}_{HG}(g;\psi) \cos\psi \, d\cos\psi = g. \qquad (3.35)$$

The graphical representation of this equation is shown below:

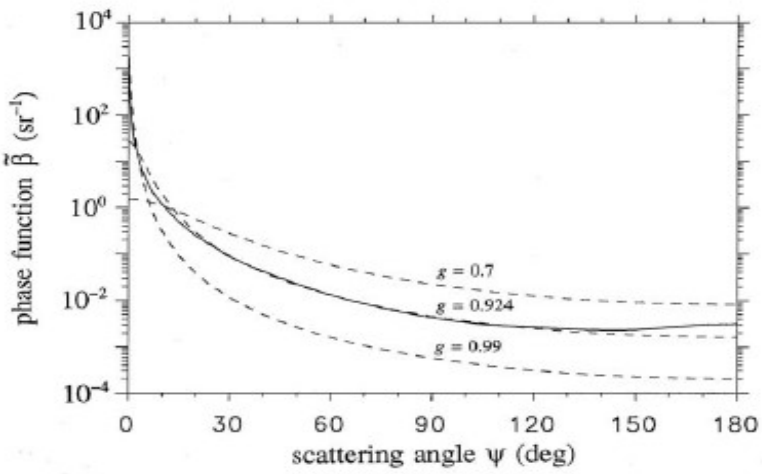

Fig. 3.15 Comparison of the particle phase function $\tilde{\boldsymbol{\beta}}_p$ from Fig. 3.13(b) (solid line) with $\tilde{\boldsymbol{\beta}}_{HG}$ of Eq. (3.34) for three values of g (dashed lines).

for a wavelength of 514 nm

While this equation was used until the end of the 20th century, it has since been replaced by an updated version that provides a better match with observations, especially for smaller scattering angles. The initial version was by Fournier-Forand (1994) with the latest update by Fournier and Jonasz (1999):

Fig. 1. Log-log plot of the Fournier-Forand phase functions for selected backscatter fractions. The green curve is the pure sea water phase function, which has .

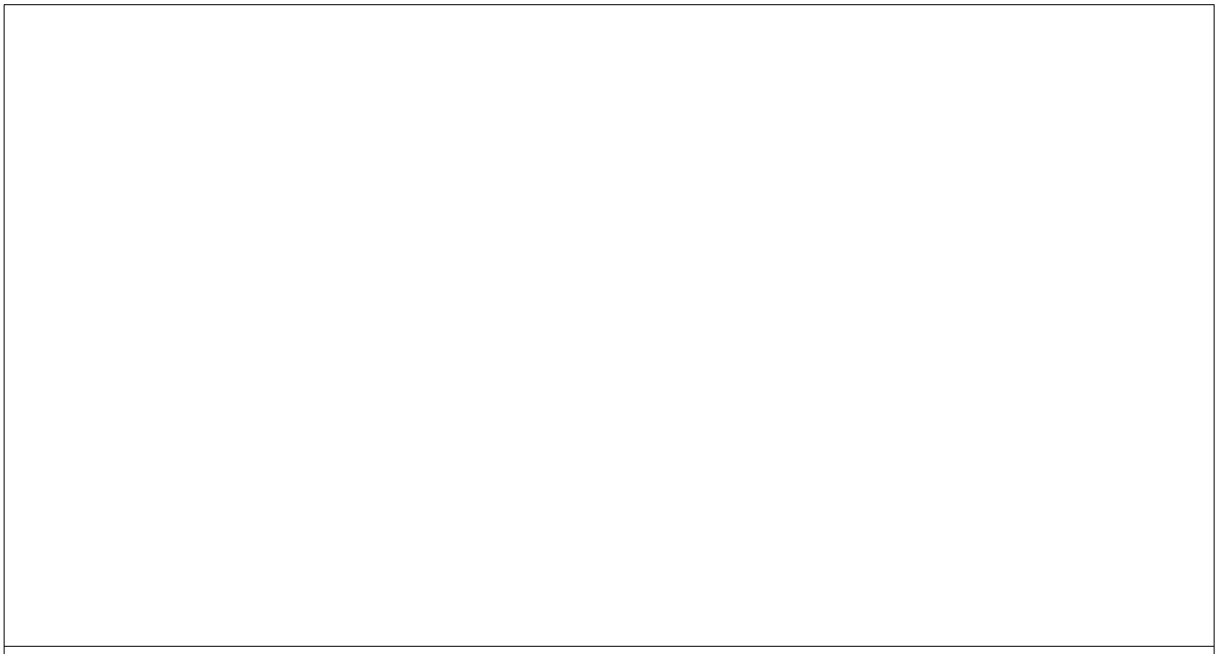

Fig. 2. Log-linear plot of the Fournier-Forand phase functions for selected backscatter fractions . The green curve is the pure sea water phase function, which has

For additional information see
http://www.oceanopticsbook.info/view/scattering/the_fournierforand_phase_function

Note that these graphs correspond to a certain wavelength. In optical oceanography you need to measure these curves at all visible wavelengths. The variability due to the different types of particles present in the water is highlighted using some biological examples below.

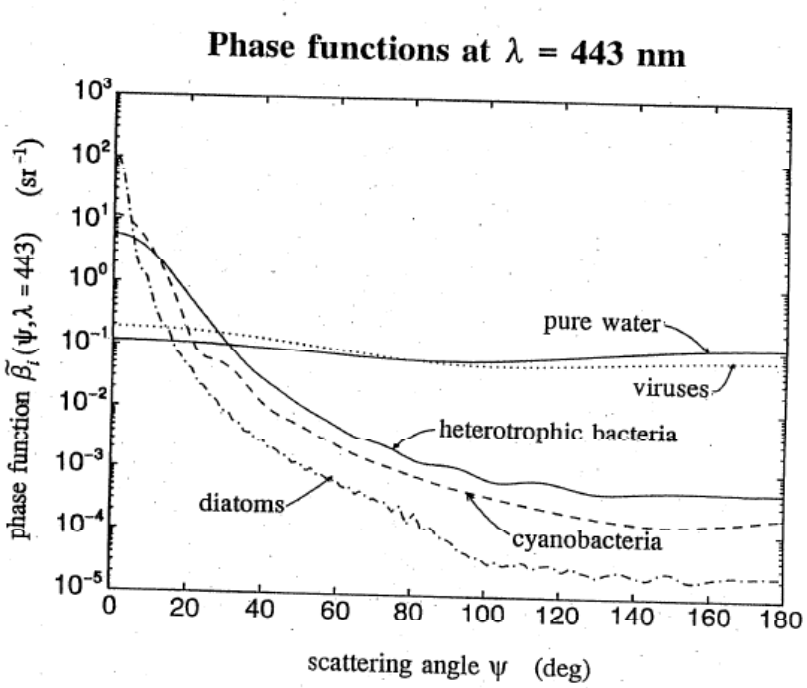

A size-based model dividing particles into small and large size categories has been proposed by Kopelevitch (1983); reformulated in 1991 by Haltrin and Kattawar.

$$b(\lambda) = b_w(\lambda) + b_{ps}^{\circ}(\lambda)P_s + b_{pl}^{\circ}(\lambda)P_l . \qquad (3.43)$$

Here $b_w(\lambda)$ is given by

$$b_w(\lambda) = 5.826\times10^{-3}\left(\frac{400}{\lambda}\right)^{4.322}, \qquad (3.44)$$

which is essentially the same as Eq. (3.31) and the data in Table 3.8. The terms $b_{ps}^{\circ}(\lambda)$ and $b_{pl}^{\circ}(\lambda)$ are the specific scattering coefficients for small and large particles, respectively, and are given by

$$b_{ps}^{\circ}(\lambda) = 1.1513\left(\frac{400}{\lambda}\right)^{1.7} \quad (\mathrm{m^2 g^{-1}})$$

$$b_{pl}^{\circ}(\lambda) = 0.3411\left(\frac{400}{\lambda}\right)^{0.3} \quad (\mathrm{m^2 g^{-1}}).$$

P_s and P_l are the concentrations in g m^{-3} of small and large particles, respectively. These quantities are parameterized in terms of the chlorophyll concentration C, as shown in Table 3.14. This work also presents a model for

Table 3.14. Parameterization of the concentrations of small (P_s) and large (P_ℓ) particles in terms of the chlorophyll concentration C, for use in Eqs. (3.43) and (3.45).[a]

C (mg m^{-3})	P_s (g m^{-3})	P_ℓ (g m^{-3})
0.00	0.000	0.000
0.03	0.001	0.035
0.05	0.002	0.051
0.12	0.004	0.098
0.30	0.009	0.194
0.60	0.016	0.325
1.00	0.024	0.476
3.00	0.062	1.078

[a] Reproduced from Haltrin and Kattawar (1991), with permission.

In addition, several simple models have been proposed to obtain the scattering function based on, for instance, the amount of chlorophyll in the water.

$b(\lambda)$. A commonly employed bio-optical model for $b(\lambda)$ is that of Gordon and Morel (1983):

$$b(\lambda) = \left(\frac{550}{\lambda}\right) 0.30 C^{0.62} \qquad (\mathrm{m}^{-1}). \tag{3.40}$$

Here λ is in nm, and C is the chlorophyll concentration in mg m^{-3}. This model includes the contribution of pure water to the total scattering; this contribution is negligible except at very low chlorophyll values. Morel (1991b) adds a pure-water term, $b_w(\lambda)$, to the right-hand side of Eq. (3.40), so that the model gives the correct value at $C = 0$. We shall use this model in Section 11.8.

A related bio-optical model for the total backscatter coefficient $b_b(\lambda)$ is found in Morel (1988; see also Stramski and Kiefer, 1991):

$$b_b(\lambda) = \tfrac{1}{2} b_w(\lambda) + \left[0.002 + 0.02\left(\tfrac{1}{2} - \tfrac{1}{4}\log C\right)\left(\frac{550}{\lambda}\right)\right]\left[0.30 C^{0.62} - b_w(550)\right]. \tag{3.41}$$

Backscattering by particles

The spectral slope of particle backscattering (often denoted as gamma) increases as the percentage of small particles increases (e.g., Reynolds et al., 2001, Stramska et al., 2003).

“The measurement of the particle backscattering coefficient, bbp, allows an estimate of the particle load in an open ocean water column. Together with fluorescence measurements of chl, it yields a proxy for particulate carbon concentrations. Although its measurement is affecgted by the refractive index and the particle size (Stramski et al., 2004), the fluo(chl)/bbp ratio makes it possible to identify photo-acclimation (Nencioli, 2010; Barbieux, 2014), possible nutritional stress (Cleveland and Perry, 1987), and differentiate between different phytoplankton communities (Nencioli, 2010; Cetenik et al. 2012). The use of these two parameters makes it possible to estimate the deep chlorophyll maxima (DCM) associated with deep biomass maxima (DBM) (Cullen, 2015).” (Extract adapted from Cornec, Stage M2 MIO, 2018).

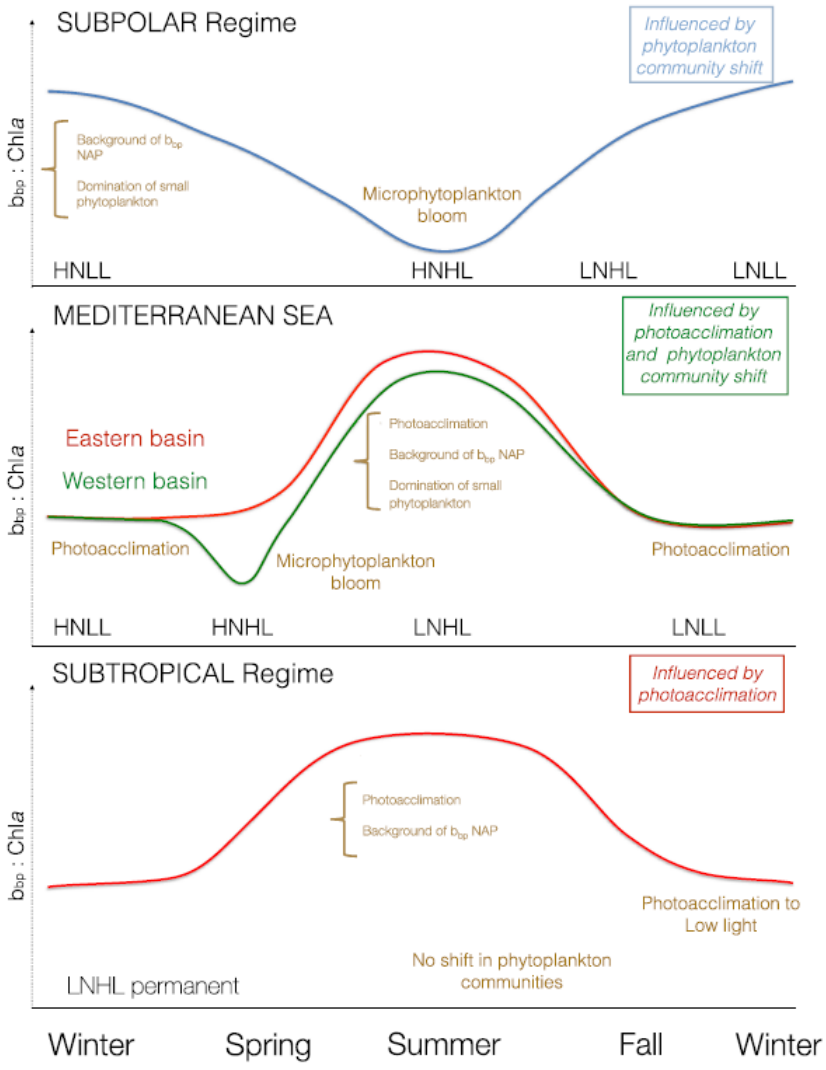

Figure 8. Conceptual scheme of the seasonal cycle of the b_{bp}:Chl*a* ratio in the surface layer of the ocean with potential factors explaining its variability. HNLL, High Nutrient Low Light; HNHL, High Nutrient High Light; LNHL, Low Nutrient High Light; LNLL, Low Nutrient Low Light.

Barbieux, M., Uitz, J., Bricaud, A.,Organelli, E., Poteau, A.,Schmechtig, C., Claustre, H. (2018). Assessing the variability in the relationship between the particulate backscattering coefficient and the chlorophyll a concentration from a global Biogeochemical-Argo database. Journal of Geophysical Research: Oceans, 123. https://doi.org/10.1002/ 2017JC013030

Note:
It is important to note that the absorption and scattering measurements may be uncorrelated. They both need to be measured or modelled. There are also approaches that try to model the sum of absorption and scattering, i.e., attenuation.

Voss (1992) has developed an empirical model for $c(\lambda)$ given a measurement of c at $\lambda = 490$ nm:

$$c(\lambda) = c_w(\lambda) + [c(490) - c_w(490)][1.563 - 1.149\times10^{-3}\lambda], \quad (3.47)$$

where λ is in nm and c is in m^{-1}. The attenuation coefficient for pure sea water, $c_w = a_w + b_w$, is given by the Smith-Baker data of Table 3.5. This model was statistically derived from data of global extent. Testing of the model with independent data usually gave errors of less than 5%, although occasional errors of ~20% were found.

Voss also determined a least-squares fit of $c(490)$ to the chlorophyll concentration. The result,

$$c(490) = c_w(490) + 0.39C^{0.57}, \quad (3.48)$$

It is not trivial to obtain the terms of absorption, scattering, and attenuation associated with the different constituents of sea water. The reverse approach, i.e., trying to identify the different constituents from measurements of a, b and c is also far from trivial. This is called solving the problem with a "**reverse approach**".

Efforts have been made to create databases, for example:

Organelli Emanuele, Barbieux Marie, Claustre Hervé, Schmechtig Catherine, Poteau Antoine, Bricaud Annick, Uitz Julia, d'Ortenzio Fabrizio, Dall'olmo Giorgio (2016). A global bio-optical database derived from Biogeochemical Argo float measurements within the layer of interest for field and remote ocean color applications. **SEANOE**. http://doi.org/10.17882/47142

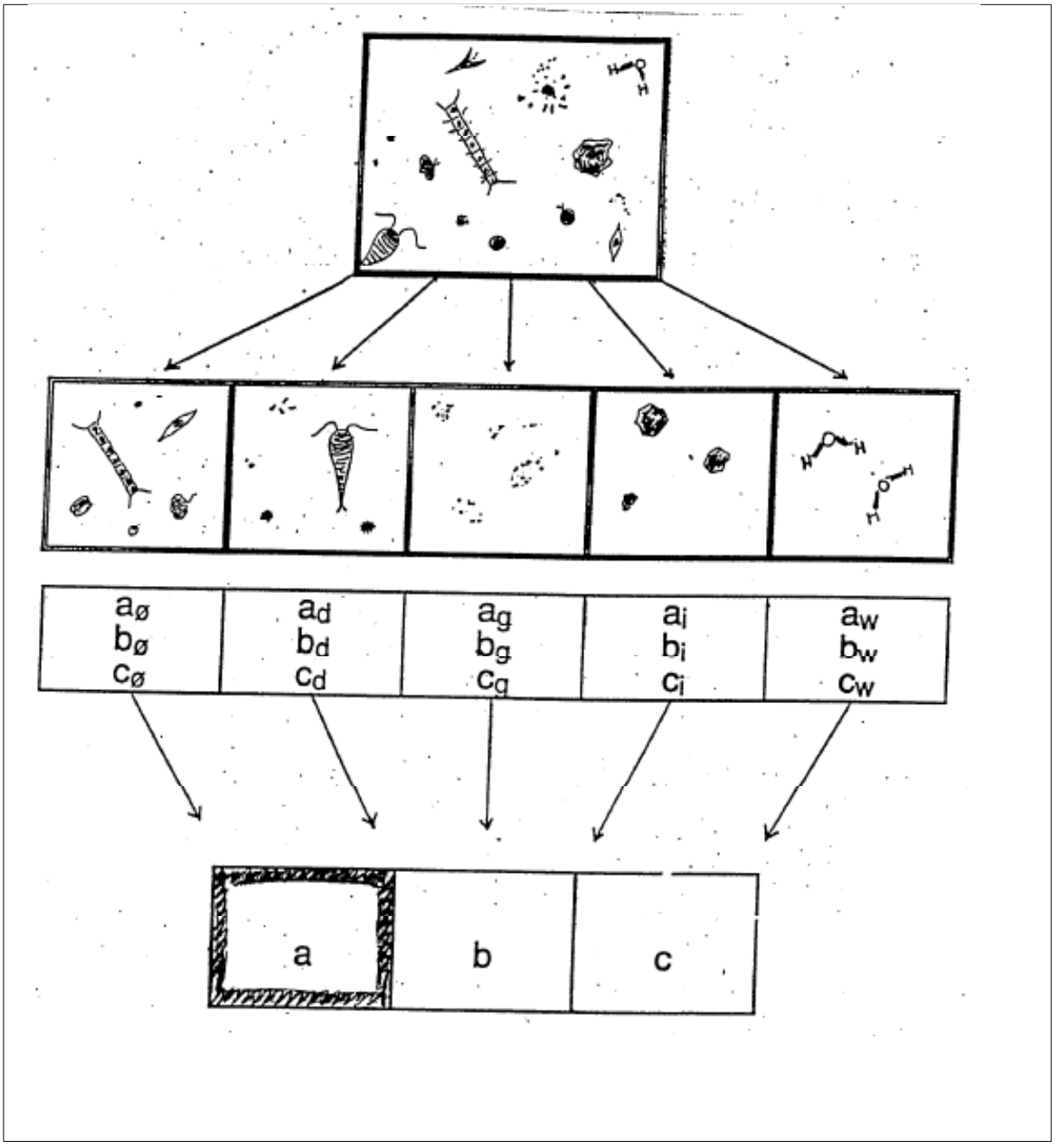
aø
bø
cø
ad
bd
cd
ag
bg
cg
ai
bi
ci
aw
bw
cw
a
b
c

C) Treating the phenomenon from an energy point of view

Absorption
At the photon level (light quanta), absorption represents the phenomenon by which the energy of a photon is taken by another particle, for example, an atom whose valence electrons make a transition between 2 energy levels. The photon is destroyed by this operation and the electromagnetic energy is absorbed and transformed into "electronic" energy.

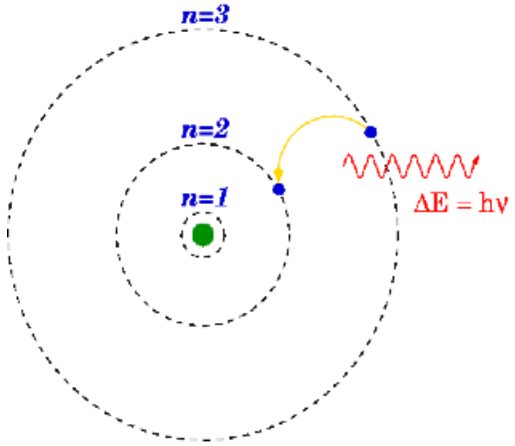

Absorption only occurs if the energy of the photon is equal to the energy difference between the energetic ground state of an atom or molecule and one of its excited states (in order of decreasing energy requirements to achieve a transition we distinguish between electronic, vibrational, oscillatory, and translational transitions).

This absorbed energy can then be used for photosynthesis, be re-transformed into electromagnetic energy by the emission of one or several photons, or be transformed into vibrational energy (increase in the speed of the particle) which, at the macroscopic level, results in an increase in temperature (electromagnetic energy has been transformed into heat).

Application to photosynthetic pigments
When the energy accumulated in the pigment molecule is released during the return of the molecule to its ground state, there are three ways of releasing this energy (apart from converting it into heat):

- through fluorescence,
- through transition to another energetic state,
- by using the energy to modify the chemical structure of the pigment or of a neighbouring molecule (this process corresponds to photosynthesis).

There are two main types of photosynthetic pigments: (i) active pigments capable of releasing the received light energy in either of the three aforementioned ways, and (ii) accessory pigments unable to carry out any energy conversion.

- active pigments (Chlorophyll *a*, Bacteriochlorophyll)
- accessory pigments (Carotene - orange; Chlorophyll *b* - yellow-green; Xanthophyll – yellow, and Phycobiliproteins - forming an antenna called the "photosynthesis collecting antenna")

Accessory pigments can “transmit” (via magnetic resonance) the captured energy to the

photosynthetic centres. Photosynthesis uses the lowest energy level of the visible spectrum (equivalent to a red photon) regardless of colour of the photon absorbed (any excess energy of the absorbed photon is released otherwise). This is why PAR can be used to derive the radiation available for photosynthesis although it is in fact a measure of the number of photons available.

Scattering

There are two types of scattering:

- elastic scattering with $\Delta t = 10^{-20}$ s

where the photon only changes direction (except for direct forward scattering with $\psi = 0°$) but not its wavelength

- inelastic scattering with $10^{-20}\text{s} < \Delta t < 10^{-7}\text{s}$

where the photon's wavelength changes. Generally, the newly emitted photon has a longer wavelength.

There are two types of inelastic scattering:

- Raman scattering with $\Delta t = 10^{-20}$ s (polarised)
  It is caused by water molecules and can both increase or decrease the wavelength of the scattered photon.
- fluorescence with $10^{-11}\text{s} < \Delta t < 10^{-7}\text{s}$ (non polarised)

From a physics point of view, the time interval for fluorescence is rather long. Fluorescence can in fact be considered as absorption followed by the emission at a different wavelength.

Phosphorescence is an even slower form of fluorescence with time intervals ranging from 10^{-3}s to a full day (e.g., the small adhesive plastic stars that are used to create the illusion of a starry sky at night).

Note: be careful not to confuse this with bioluminescence which is the ability to emit light due to an enzymatic reaction involving oxygen and two key molecules: luciferin and luciferase. This process, unlike fluorescence and phosphorescence, does NOT require the object to be excited by a light source, neither in the moment nor beforehand.

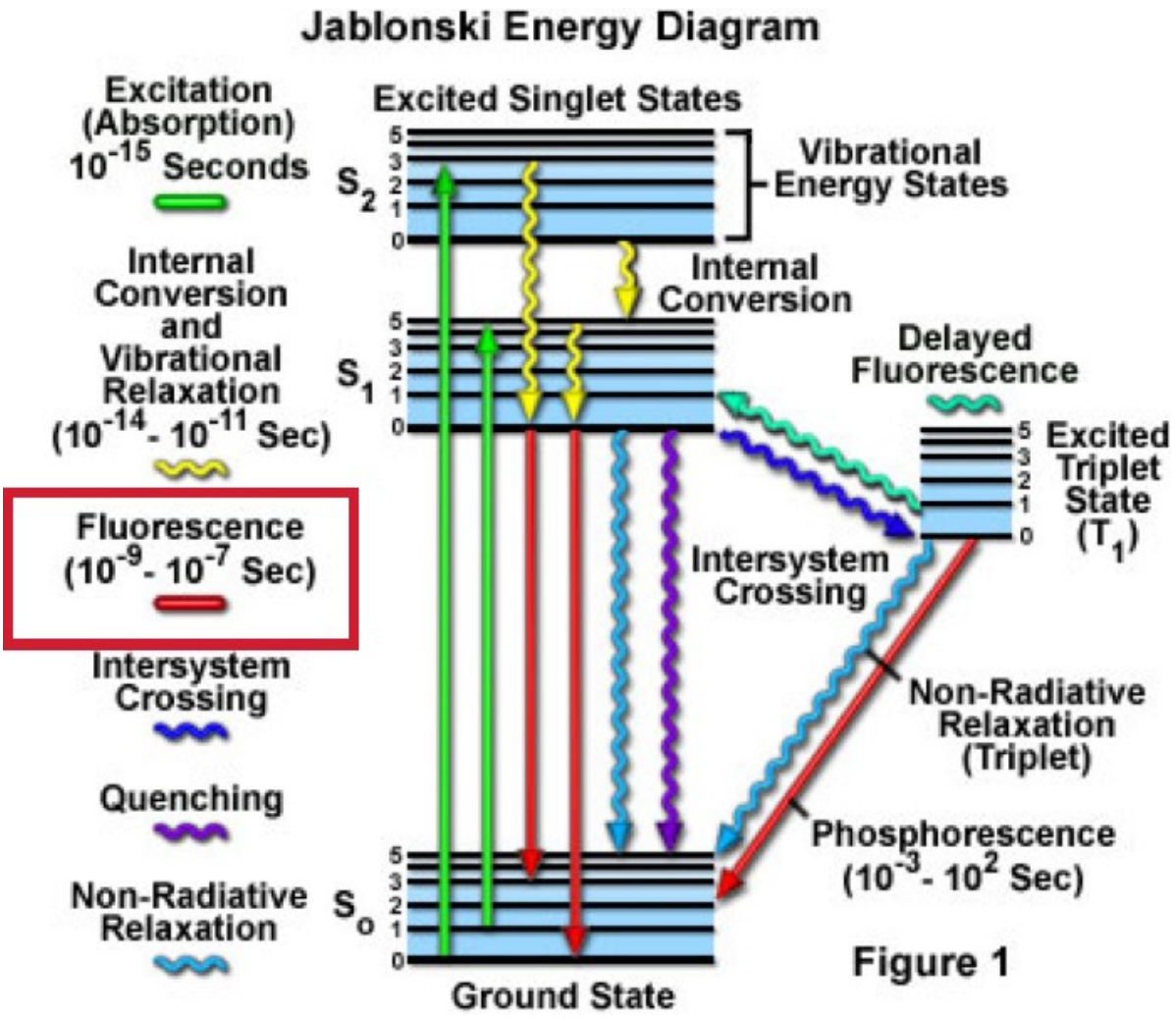

http://micro.magnet.fsu.edu/primer/java/jablonski/jabintro/index.html
http://www.micro.magnet.fsu.edu/primer/java/fluorescence/exciteemit/index.html

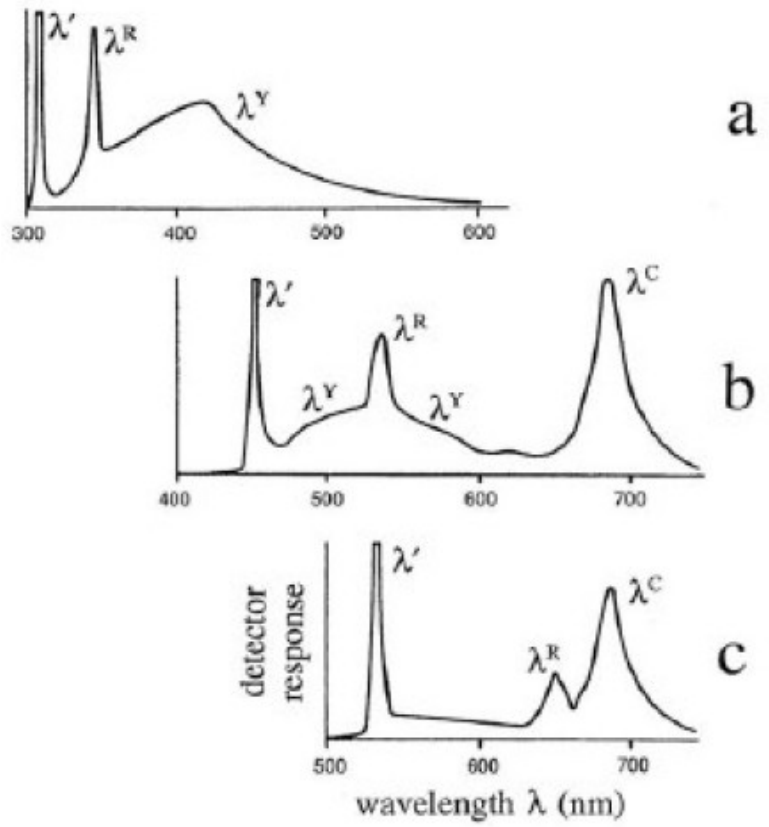

Fig. 5.9. Response of a water sample from the North Sea to excitation at three different wavelengths, λ'. The symbol λ^R identifies the Raman band, λ^Y fluorescence by yellow matter, and λ^C fluorescence by chlorophyll. [redrawn from Diebel-Langohr, *et al.* (1986), by permission]

Excitation wavelengths λ' used were a) 308 nm, b) 450 nm and c) 533 nm.
The Raman scattering wavelengths are respectively a) 344 nm, b) 533 nm, and c) 650 nm.

Fluorescent compounds are excited (i.e., can absorb light) at one or several wavelengths, but always fluoresce at the same wavelength.

Three examples (chlorophyll *a*, tryptophan, pyrene)

a) Example of chlorophyll fluorescing at two pairs λEx/λEm:
λEx1/λEm = 430/672 nm and λEx2/λEm = 656/672 nm

The excitation spectrum is obtained by measuring the fluorescence at the fixed emission wavelength (in this case 672nm) while varying the excitation wavelength from 220 to 700nm.

The emission spectrum is obtained by measuring the fluorescence at a fixed excitation wavelength (in this case 416nm) while varying the emission wavelength from 600 to 800nm.

There is a second excitation peak at 656 nm for chla that is never used by the fluorescence probes who normally use the pair Ex/Em of 430/672 nm (or similar nearby pairs; see course OPB201 Petrenko).

b) Example of tryptophan fluorescing at 2 pairs:
λEx1/λEm = 225/350 nm and λEx2/λEm = 275/350 nm
(see the application for urban waste plume detection in Petrenko et al, JGR, 1997)

- Example 1: excitation spectrum obtained at fixed emission wavelength of 350 nm while varying the excitation wavelength from 220 to 400 nm (two peaks are detected at 225 and 275 nm)
- Example 2: emission spectrum obtained at fixed excitation wavelength of 225 or 275 nm while varying the emission wavelength from 250 to 550 nm (we detect a peak at 350 nm).

c) Examples for pyrene:
- excitation spectrum obtained for a fixed emission wavelength of 380 nm while varying the excitation wavelength from 220 to 400 nm (we detect 3 peaks at 240, 270, and 335 nm)
- emission spectrum obtained for fixed excitation wavelengths of 240, 270, or 335 nm while varying the emission wavelength from 300 to 550 nm (we detect a peak at 380 nm)

• **Chlorophylle *a*** → indice de biomasse phytoplanctonique

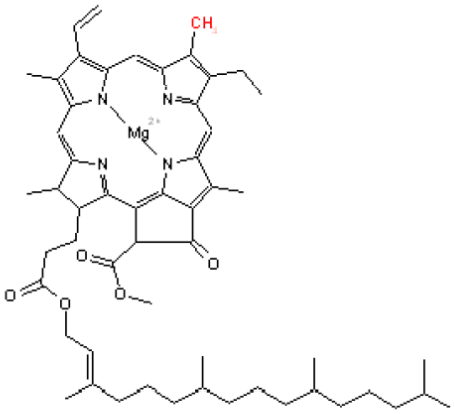

λEx1/λEm = 430/672 nm

λEx2/λEm = 656/672 nm

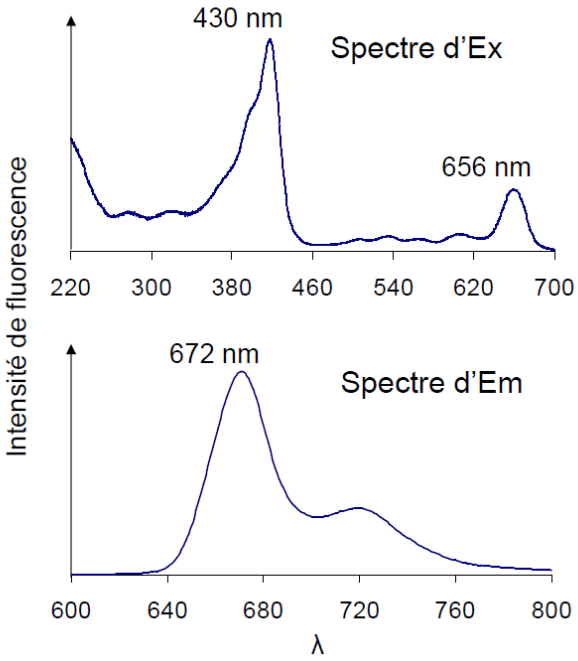

• **Tryptophane** → produit du phytoplancton / indicateur de contamination en eaux usées (Petrenko et al., 1997)

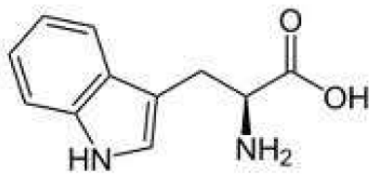

λEx1/λEm = 225/350 nm

λEx2/λEm = 275/350 nm

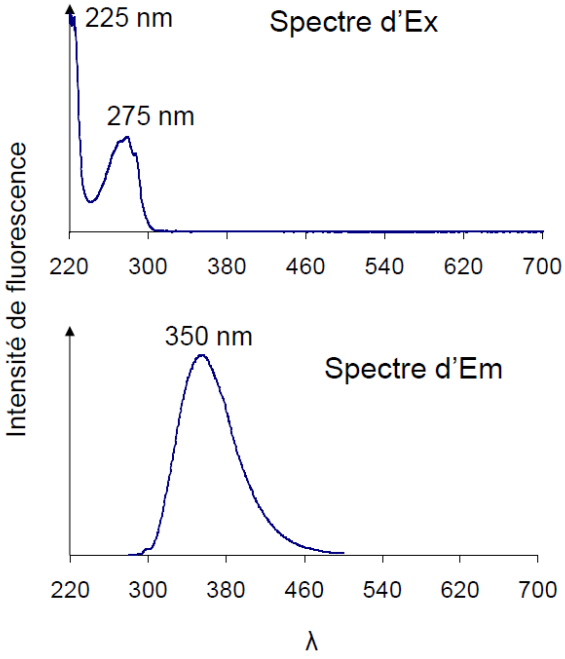

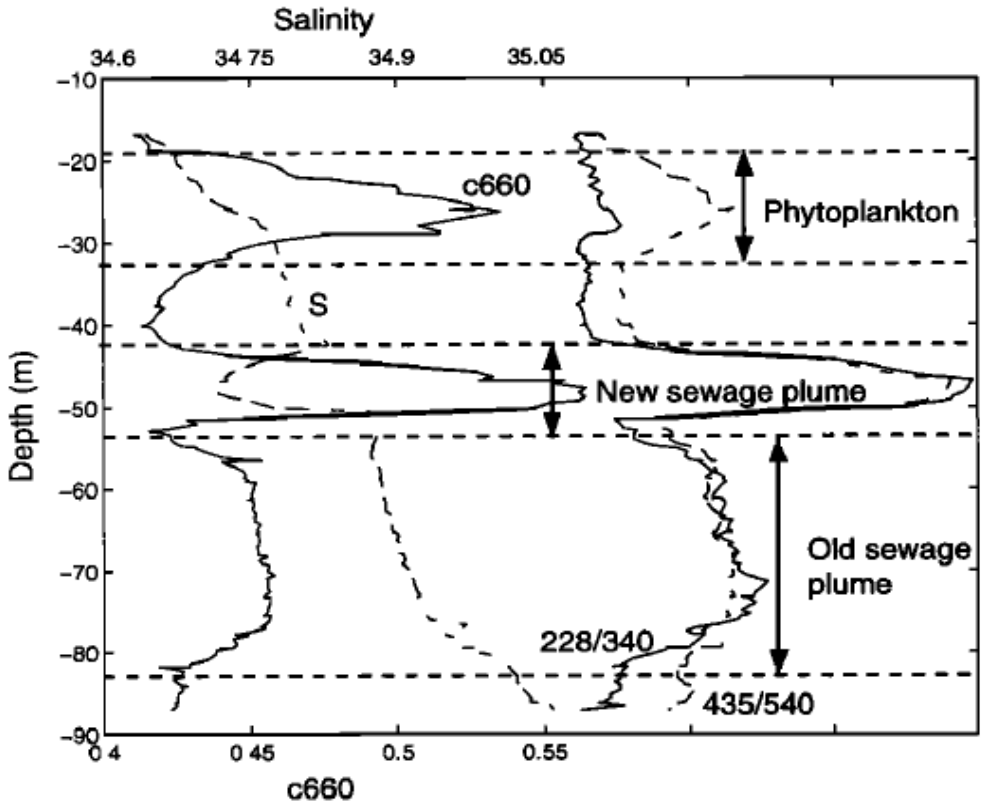

Figure 2. Profiles of salinity, beam attenuation coefficient at 660 nm (c660), and fluorescence, in arbitrary units, for Ex/Em = 228/340 nm and Ex/Em = 435/540 nm. Data are from the second downcast of towyo 32. Three layers were observed: shallow phytoplankton, new and old sewage plumes.

Miniature optical sensor installed on MIO's the SEAExplorer glider (MIO PIs M Goutx and M. Tedetti);
Cyr et al., (2017). *A new glider-compatible optical sensor for dissolved organic matter measurements: test case from the NW Mediterranean Sea.* Front. Mar. Sci., 4:89, doi:10.3389/fmars.2017.00089 (see publications on the homepage of A. Petrenko)

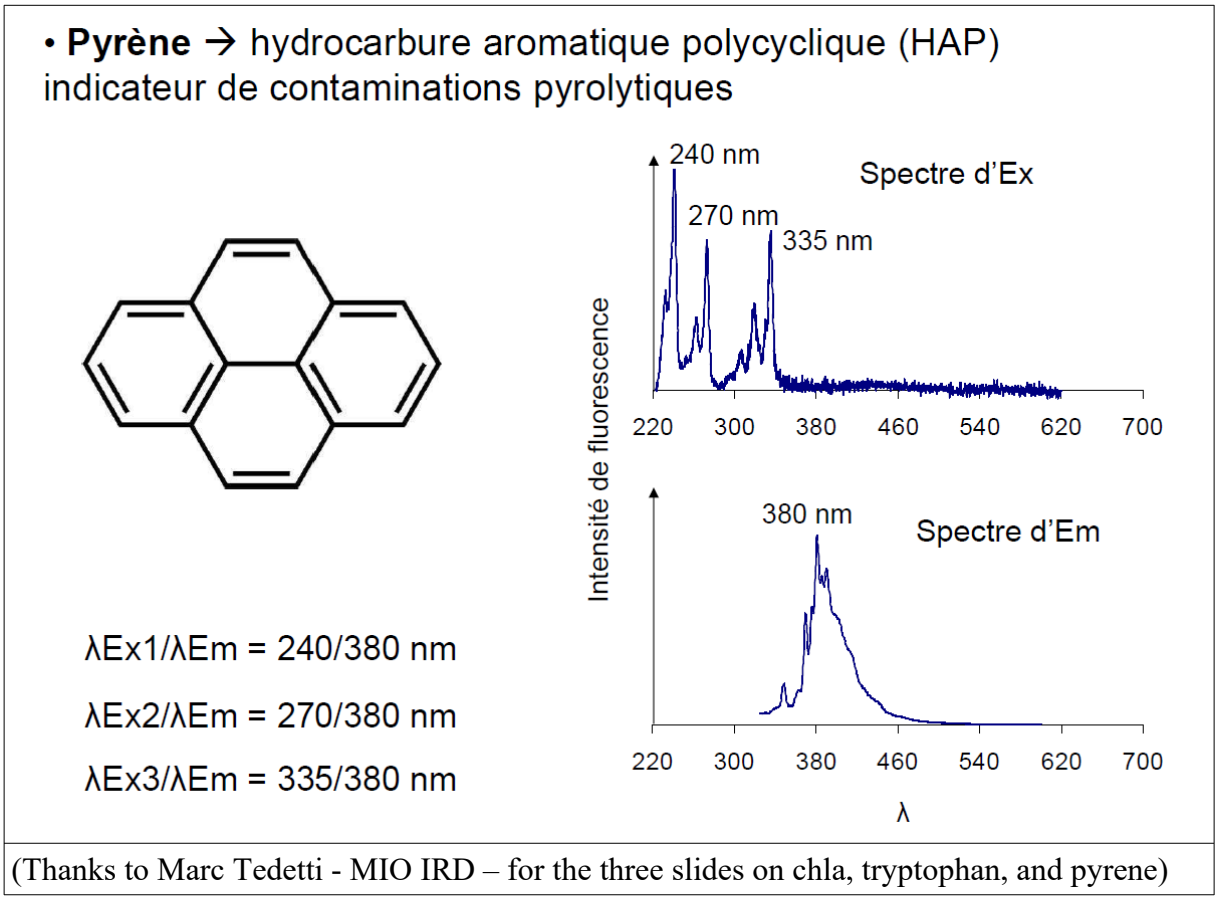

(Thanks to Marc Tedetti - MIO IRD – for the three slides on chla, tryptophan, and pyrene)

Historical note: In 2008, three scientists (Roger Tsien, UCSD, Martin Chalfie, Columbia Univ., and Osama Shimomura, Japan) received the Nobel Price in chemistry for their research on the gene of the protein responsible for green fluorescence. This gene was given to them by Douglas Prasher (then at WHOI).

Bibliography

Cetinić, I., Perry, M. J., Briggs, N. T., Kallin, E., D'Asaro, E. A., & Lee, C. M. (2012). Particulate organic carbon and inherent optical properties during 2008 North Atlantic Bloom Experiment. *Journal of Geophysical Research: Oceans*, *117*(C6).

Cetinić, I., Perry, M. J., D'asaro, E., Briggs, N., Poulton, N., Sieracki, M. E., & Lee, C. M. (2015). A simple optical index shows spatial and temporal heterogeneity in phytoplankton community composition during the 2008 North Atlantic Bloom Experiment. *Biogeosciences*, *12*(7), 2179-2194.

Cleveland, J. S., & Perry, M. J. (1987). Quantum yield, relative specific absorption and fluorescence in nitrogen-limited Chaetoceros gracilis, *Mar. Biol.*. 94:489.

Nencioli, F., Chang, G., Twardowski, M., & Dickey, T. D. (2010). Optical characterization of an eddy-induced diatom bloom west of the island of Hawaii. *Biogeosciences*, *7*(1), 151-162.

Cullen, J. J. (2015). Subsurface chlorophyll maximum layers: enduring enigma or mystery solved?. *Annual review of marine science*, *7*, 207-239.

Stramski, D., Boss, E., Bogucki, D., & Voss, K. J. (2004). The role of seawater constituents in light backscattering in the ocean. *Progress in Oceanography*, *61*(1), 27-56.

Appendix – Extract from the thesis by Marie Barbieux (supervised by A. Bricaud and J. Uitz,

defended in 2019) – “Zoom sur les cycles diurnes”.

Measurements of chlorophyll *a* fluorescence and bio-optical properties of the ocean

Studying the distribution and sources of variability of phytoplankton biomass represents a real challenge in oceanography because this phytoplankton biomass is particularly difficult to measure. Very often, indirect measures are used. While cell counting and the conversion of biovolume to carbon biomass using empirical relationships (Strathmann 1967) are commonly used, chromatographic pigment analyses (using HPLC - "High Performance Liquid Chromatography") is the most frequently used approach to characterize phytoplankton communities. At present, it is the most precise method available and considered the reference method for quantifying chla concentration (Jeffrey & Mantoura, 1997; Roy et al., 2011), the most commonly used proxy of phytoplankton biomass. Recently, Graff et al. (2012 & 2015), coupling flow cytometry measurements and quantification of cellular carbon content, have proposed a method for the direct measurement of phytoplankton biomass. However, this method remains rather laborious and requires a substantial sampling effort to understand the variability of phytoplankton biomass at large spatio-temporal scales. This method, like all the aforementioned methods as well, is based on discrete samples.

In order to overcome the limitations inherent in discrete measurements, attention has shifted to measuring the optical properties related to phytoplankton which can be sampled continuously. Chla fluorescence (Lorenzen 1966) is still the most frequently used parameter today to estimate the concentration of chla and thus phytoplankton biomass. Chla fluorescence provides an estimate of the chla concentration, which is itself a proxy for phytoplankton biomass. However, it is not easy to directly relate chla fluorescence to phytoplankton biomass. The are several assumptions underlying the chain of proxies from fluorescence via chla to phytoplankton biomass that must be taken into account in order to correctly interpret the final estimate of the biogeochemical quantity based on the measured optical signal. The relationship between chla fluorescence and chla and between chla and the carbon content is subject to a high degree of variability. First, the fluorescence/chla ratio varies depending on the phytoplankton communities present in the sample, their acclimation to light, nutrient levels, the growth phase of phytoplankton cells, and the amount of nonphotochemical quenching (Cullen 1982; Geider et al. 1998; Proctor & Roesler 2010; Macintyre et al. 2011). Similarly, the carbon/chla ratio fluctuates not only between species but also within the same species depending on environmental conditions (Banse 1977; Geider 1987; Cloern et al. 1995) and growth phases (Riemann et al. 1989; Geider et al.1997).

In order to better constrain the conversion from chla fluorescence to phytoplankton biomass, it is possible to use additional measurements of inherent optical properties (IOPs) such as the particle backscattering (b_{bp}) or attenuation (c_p) coefficient which provide additional information on the types of particle. These optical properties provide information primarily about the abundance but also about the nature of the particles present in the sample (e.g., micro-organisms, non-living particles) (Morel & Bricaud 1986; Babin et al. 2003; Huot et al. 2007; Whitmire et al. 2010). Moreover, b_{bp} and c_p are less dependent on the physiological state (response to light and nutrients) of the phytoplankton cells than measurements of chla fluorescence. On the downside, these optical indices integrate over all particles present in the sample and do allow phytoplankton to be singled out from other particles present in the sample (e.g., zooplankton, detritus, bacteria, mineral particles). The backscattering and attenuation coefficients are considered proxies of the

POC (Stramski et al. 1999; Bishop et al. 1999; Gardner et al. 2006; Cetinić et al. 2012). Finally, while neither chla fluorescence nor IOPs allow for highly accurate estimates of phytoplankton biomass on their own, we can combine them to improve the accuracy and our understanding of this key variable the oceanic carbon cycle (Behrenfeld & Boss 2003; Behrenfeld & Boss 2006; Westberry et al. 2010; Graff et al. 2015).

In addition to phytoplankton biomass, these measurements also make it possible to estimate the amount of primary production (from chla) and community production (measurements of IOPs). In fact, these measurements can be used as input variables in bio-optical models of "primary production" (PP). These types of models also require the amount of irradiance available for photosynthesis as input variable and can be coupled with satellite observations of ocean colour tp obtain overall estimates of PP (Longhurst et al. 1995; Antoine et al. 1996; Behrenfeld & Falkowski 1997; Uitz et al. 2010). However, many photophysiological parameters in these models remain poorly constrained due to the lack of relevant *in situ* data (Babin et al. 1994; Sakshaug et al. 1997; Uitz et al. 2008). The small number of *in situ* measurements of PP in the global ocean also hampers the validation of global PP estimates (e.g., Marra 2015; Siegel et al. 2016).
In this context, the use of the diurnal cycles in IOPs could constitute an interesting alternative for estimating production (Siegel et al. 1989; Claustre et al. 2008; Gernez et al. 2011). The particle backscattering and attenuation coefficients show a marked diurnal cycle, characterized by an increase during the day and a decrease during the night (e.g., Gernez et al. 2011; Kheireddine & Antoine 2014; Barnes & Antoine 2014). The increase during the day is due to primary production being compensated by losses (e.g., respiration, grazing) while the nocturnal decrease is attributed to metabolic losses which dominate in the absence of autotrophic production. From these diurnal variations in optical properties, it is thus possible to quantify the production of organic carbon (e.g., Siegel et al. 1989).

The chla concentration and IOPs are thus suitable variables to investigate the spatio-temporal dynamics of phytoplankton biomass and quantify of the amount of PP in a phytoplankton community. They have the advantage that they can be measured continuously and *in situ* thanks to miniature sensors that can be mounted onto a wide range of oceanographic platforms (oceanographic vessel via a FerryBox or "continuous surface" type assembly, fixed mooring, AUV or glider, Argo float).

The diurnal cycle of inherent optical properties

The day-night cycle constitutes the main forcing of the biological activity in oligotrophic systems (e.g., Oubelkheir & Sciandra 2008). The effects of the diurnal cycle of light have been observed in the abundances of microorganisms (Jacquet et al. 1998; Vaulot & Marie 1999; Brunet et al. 2007), in chla fluorescence (Stramska & Dickey 1992; Dandonneau & Neveux 1997), or in optical properties such as the attenuation (e.g., Siegel et al. 1989) and particle backscattering coefficients (e.g., Kheireddine et Antoine, 2014, Barnes et Antoine, 2014).
Since micro-algae depend on light to photosynthesise they have adapted to this diurnal cycle. Severla studies have shown that phytoplankton cell generation and division exhibit diurnal periodicities (Chisholm & Costello 1980; Chisholm & Brand 1981; Vaulot et al. 1995) as does the intracellular chla content (Owens et al. 1980; Ohi et al. 2005; Ragni & D'Alcalà 2007), and nutrient uptake rates (Vincent 1992; Clark et al. 2002).

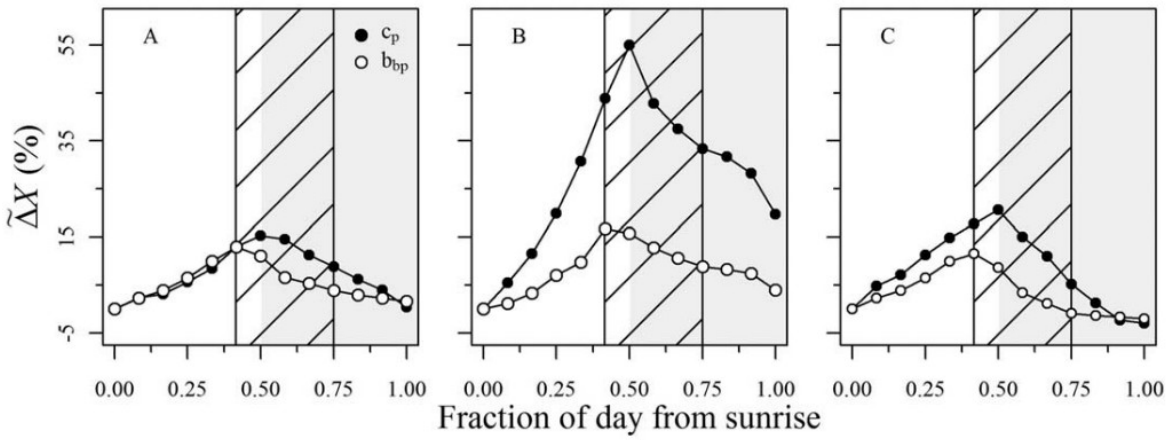

Figure 5.1: Diurnal variability of c_p (black) and b_{bp} (white) during (A) an oligotrophic period in summer, (B) a bloom, and (C) the decline of a bloom at station BOUSSOLE in the Mediterranean. The hatched part represents daylight hours while the shaded areas represent night time. Source: Kheireddine & Antoine, 2014.

The diurnal cycle of b_{bp} and c_p is characterized by an increase of both parameters during daytime and a decrease at night (Gernez et al. 2011; Kheireddine & Antoine 2014; Barnes & Antoine 2014) (Figure 5.1). To a first order, this daytime increase is due to the increase in cell size and abundance and, to a second order, to a change in their shape and refractive index (Stramski & Reynolds 1993; Durand & Olson 1996; Claustre et al. 2002; Durand et al. 2002). The night time decrease is due to a shrinking size and decreasing refractive index of the cells, due to respiration and cell division (Gernez 2009). However, the attenuation and backscattering coefficients do not only depend on phytoplankton but on the entire assemblage of particles present in the water column. The diurnal variability seen in these parameters is thus not exclusively related to diurnal cycles in phytoplankton physiology. Small grazers, heterotrophic bacteria, and photo-heterotrophs also contribute to this diurnal variability of the optical properties (Claustre et al. 2008; Oubelkheir & Sciandra 2008). In addition, processes such as particle aggregation and sedimentation also cause some diurnal variability. At night, the reduction in c_p and b_{bp} reflects indirectly the grazing by zooplankton (Cullen et al. 1992) and/or the dilution of particle assemblages due to the nocturnal deepening of the surface mixing layer (Gardner et al. 1995).

Same mayor results of her thesis:

Analysis of the variability and re-assessment of the b_{bp}-Chl*a* relationship

This study examined the regional, vertical, and temporal variability of the b_{bp}-Chl*a* relationship on a global scale. While the existence of a covariation between b_{bp} and Chl*a* has long been known (Smith & Baker 1978; Reynolds et al. 2001; Stramska et al. 2003; Huot et al. 2008; Antoine et al. 2011; Xing et al. 2014), the spatio-temporal variability of this relationship remained poorly understood. In this study, we re-evaluated the global relationship between b_{bp} and Chl*a*. First, we pointed out some general trends before examining second order variabilities which allowed us to identify regional differences in the b_{bp}-Chl*a* relationship. Our study revealed a significant seasonal variability of the relationship between b_{bp} and Chl*a* that was aslo dependent on the layer in the water column and the geographical location. By elucidating the coupling between the amount of POC and chl*a* concentration, this study also allowed for a better characterization of the dynamics of phytoplankton biomass in different oceanic regimes across the globe. Our results show the existence of a permanent covariation between b_{bp} and Chl*a* in the surface layer of subpolar gyres and a decoupling of these two parameters in oligotrophic regions of the global ocean.
At large spatio-temporal scales and to a first order of variability, we recommend the use of the b_{bp}:Chl*a* ratio to characterize the concentration and nature (composition and size) of particle assemblages in SPGs (Subpolar Gyres) and the Western Mediterranean Basin, i.e., in so-called “biomass” regimes. In contrast, the b_{bp}:Chl*a* ratio can be used as a photophysiological index in STGs (Subtropical Gyres) and the Eastern Mediterranean Basin, i.e., in so-called “photoacclimation” regimes.

This study thus emphasises the strong potential of existing global databases containing data from BGC-Argo floats to re-evaluate the empirical bio-optical relationships and supply the scientific community with valuable *in situ* data. We expect our analysis to be particularly useful to the ocean colour community, as it allows parametrisation in semi-analytical bio-optical models to be improved and remotely sensed estimates of Chl*a* or b_{bp} to be validated.

Study of the seasonal and regional dynamics of subsurface Chla maxima

To the best of our knowledge, this study represents the first attempt to examine the spatio-temporal variability of subsurface chlorophyll maxima (SCMs) in the Mediterranean based on data from BGC-Argo floats equipped with light (PAR) and nitrate ($[NO_3^-]$) sensors. Although the presence of SCMs in oligotrophic regions of the global ocean has been known for decades (Cullen & Eppley 1981; Raimbault et al. 1993; Letelier et al. 2004; Mignot et al. 2014) their spatio-temporal dynamics remains very poorly documented.

The goal of the present study was to improve our understanding of the occurrence, the underlying mechanisms, and biogeochemical characteristics of SCMs in the Mediterranean Sea. In this chapter, we have identified two main types of SCM, namely:
(1) SCMs with sufficient light and nutrient availability to exhibit a real increase in biomass at depth (SBMs pour subsurface biomass maxima); and

(2) SCMs that result from an intracellular increase in chlorophyll *a* as a result of photoacclimation to low light.

Our results suggest that while SBMs are a recurring feature in the Western Mediterranean Basin, in the Eastern Basin, SCMs primarily result from photoacclimation. Thus, while seasonal cycles of surface Chl*a,* as derived from by satellites observations of ocean colour, may appear similar across many regions of Mediterranean, our results suggest that at depth, the situations can vary significantly between regions. In contrast to the idea that SCMs in oligotrophic regions typically result from photoacclimation, this study shows that SBMs are also frequently observed in the Mediterranean. As a result, we suggest that the contribution of SCMs to the overall PP could be rather significant despite them being largely ignored in current estimates derived from satellite observations.

Quantifying community production

Primary production (*i.e.* production by autotrophic micro-organisms) in the ocean is an essential component of the marine carbon cycle. Especially at a time of imminent climate change, it is important to develop new approaches that allow the PP to be quantified at high spatio-temporal resolutions and based on *in situ* measurements. Using the observed diurnal cycle in bio-optical properties as measured by BGC-Argo floats using multiple vertical profiles, we could estimate the community production (*i.e.,* the production by phytoplankton and heterotrophic bacteria) in different layers of the water column during the oligotrophic summer period in two different regions of the Mediterranean. Our estimates of community production are of the same order of magnitude as previous estimates obtained for other oligotrophic regions (*e.g*., Claustre et al. 2008). We found that the community production is lower in the Ionian Sea compared to the Ligurian Sea, as is the contribution of the SCM to the total water column production.

In the Ligurian Sea, more than 40% of the community production occurs in the SCM. This underlines the importance of taking SCMs into account in global estimates of PP. Our study of very fine spatial and temporal scales, points toward the existence of a strong spatio-temporal heterogeneity of the biological production in oligotrophic regimes, while revealing a significant impact of mesoscale (or small scale) processes on our estimates in the subsurface layers. Finally, while this study confirms that b_{bp} is not an adequate proxy to estimate the community production, it underlines the usefulness of high-resolution measurements of this parameter. In fact, if combined with measurements of other parameters such as c_p or Chl*a*, b_{bp} remains extremely useful to understand the degree of photoacclimation of phytoplankton cells and/or the structure and nature of the particle assemblages.